



Late Holocene intensification of the westerly winds at the subantarctic Auckland Islands (51° S), New Zealand

Imogen M. Browne¹, Christopher M. Moy¹, Christina R. Riesselman^{1,2}, Helen L. Neil³, Lorelei G. Curtin¹, Andrew R. Gorman¹, Gary S. Wilson^{1,2,4}

5 ¹Department of Geology, University of Otago, Dunedin, 9016, New Zealand

²Department of Marine Science, University of Otago, Dunedin, 9016, New Zealand

³National Institute of Water and Atmospheric Research (NIWA), Wellington, 6021, New Zealand

⁴New Zealand Antarctic Research Institute (NZARI), Christchurch, 8053, New Zealand

Correspondence to: Imogen M. Browne (imogenbrowne@usf.mail.edu)

10 **Abstract.**

The Southern Hemisphere westerly winds (SHWW) play a major role in controlling wind-driven upwelling of Circumpolar Deep Water (CDW) and outgassing of CO₂ in the Southern Ocean on interannual to glacial-interglacial timescales. Despite their significance in the global carbon cycle, our understanding of millennial-scale changes in the strength and latitudinal position of the westerlies during the Holocene (especially since 5,000 yr BP) is limited by a scarcity of paleoclimate records from comparable latitudes. Here, we reconstruct middle to late Holocene variability in the SHWW using a fjord sediment core collected from the subantarctic Auckland Islands (51° S, 166° E), located in the modern centre of the westerly wind belt. Drainage basin response to variability in the strength of the SHWW at this latitude is reconstructed from downcore variations in magnetic susceptibility (MS) and bulk organic δ¹³C and atomic C/N, which monitor influxes of lithogenous and terrestrial vs marine organic matter, respectively. The hydrographic response to SHWW variability is reconstructed using benthic foraminifer δ¹⁸O and δ¹³C, both of which are influenced by the isotopic composition of shelf water masses entering the fjord. Using these data, we provide marine and terrestrial-based evidence for increased wind strength from ~1,600-900 yr BP at subantarctic latitudes that is broadly consistent with previous studies of vegetation response to climate at the Auckland Islands. Comparison with a SHWW reconstruction using similar proxies from Fiordland suggests a northward migration of the SHWW over New Zealand at the beginning of the Little Ice Age (LIA). Comparison with paleoclimate and paleoceanographic records from southern South America and the western Antarctic Peninsula indicates a late Holocene strengthening of the SHWW after ~1,600 yr BP that appears to be broadly symmetrical across the Pacific basin, although our reconstruction suggests that this symmetry breaks down during the LIA. Contemporaneous increases in SHWW at localities either side of the Pacific in the late Holocene are likely controlled atmospheric teleconnections between the low and high latitudes and by variability in the Southern Annular Mode (SAM) and El Niño Southern Oscillation (ENSO).

30



1 Introduction

The Southern Hemisphere Westerly Winds (SHWW) influence mid-latitude climate and global carbon cycling on a variety of timescales. The position, strength, and symmetry of the SHWW determines precipitation patterns over mid-latitude southern landmasses, and modifies upwelling of nutrient- and carbon-rich water along oceanic fronts associated with the Antarctic Circumpolar Current (ACC; Carter et al., 2009; Dinniman et al., 2012; Lovenduski and Gruber, 2005; Menviel et al., 2008). Southern Ocean upwelling releases CO₂ into the atmosphere and provides nutrients to lower latitudes via northward advection of Subantarctic Mode Water (SAMW), which forms at the Subantarctic Front (SAF), on the northern margin of the ACC (Carter et al., 2009; Palter et al., 2010; Sarmiento et al., 2004). Westerly wind-driven upwelling therefore plays a major role in modulating Pacific Ocean primary productivity and Southern Ocean air-sea CO₂ exchange, on decadal to orbital timescales (Anderson et al., 2009; Lovenduski et al., 2008; Sigman et al., 2010; Skinner et al., 2010; Toggweiler et al., 2006).

Observations and models demonstrate that the Subantarctic Zone (SAZ), between the Subtropical Front (STF) and SAF is the largest sink for atmospheric CO₂ in the Southern Ocean (Lenton et al., 2013; McNeil et al., 2007; Metzl et al., 1999, 2006, Takahashi et al., 2002, 2012). The efficiency of the SAZ carbon sink is sensitive to decadal changes in atmospheric circulation patterns, particularly, the symmetry of low-level zonal winds (Le Quéré et al., 2007; Metzl, 2009; Takahashi et al., 2009; Landschutzer et al. 2015). A pronounced southward shift and intensification of the SHWW over the past few decades is associated with a shift towards the positive phase of the Southern Annular Mode (SAM), the dominant mode of internal climate variability in the high southern latitudes, and is thought to be impacting the efficiency of the SAZ CO₂ sink (Abram et al., 2014; Archer and Caldeira, 2008; Lovenduski et al., 2008; Marshall, 2003; Shindell and Schmidt, 2004; Thompson and Solomon, 2002). It is therefore important to constrain the zonal symmetry of the SHWW on a variety of timescales in order to understand their influence on air-sea CO₂ flux.

Although SHWW circulation is well constrained on seasonal and glacial-interglacial timescales, its behaviour on intermediate timescales remains unclear. Due to an absence of extensive continental landmasses in the Southern Hemisphere mid-latitudes, atmospheric circulation is zonally symmetric on monthly and longer time scales (Sen Gupta and England, 2006; Hall and Visbeck, 2002; Trenberth, 1991), although internal modes of climate variability such as the SAM and the El Niño Southern Oscillation (ENSO) can influence SHWW symmetry as well as regional sea surface temperatures (SSTs) (Ummenhofer et al., 2009; Ummenhofer and England, 2007). Climate data reanalysis studies demonstrate that the SHWW migrate southward in the austral summer and northward in the austral winter with a pronounced split jet over the Pacific Basin (Chiang et al., 2014; Garreaud et al., 2013; Trenberth, 1991), and a similar pattern is reconstructed on glacial-interglacial timescales, where the westerlies are shifted northward during glacials and southward during interglacials (Anderson et al., 2009; Sigman et al., 2010; Skinner et al., 2010; Toggweiler et al., 2006). Paleoclimate records indicate zonally symmetric winds from 14,000-5,000 yr BP, while a general paucity of records from comparable latitudes across the



Pacific and disagreement in interpretations of Holocene SHWW variability have precluded assessment of zonal symmetry over the past 5,000 years (Fletcher and Moreno, 2012; Kilian and Lamy, 2012; Lamy et al., 2010; Moreno et al., 2009).

65 In order to assess zonal symmetry of the winds over the middle to late Holocene, a number of well-dated and contemporaneous records of wind strength from areas influenced by the modern SHWW “core” (50-55° S), and from a range of longitudes are required. Paleoclimate records of wind strength reconstruct changes in atmospheric circulation using the strong positive correlation between wind strength and precipitation in the middle latitudes of the Southern Hemisphere (Garreaud, 2007). Although there are a number of records from southern New Zealand (Gellatly et al., 1988; Knudson et al., 70 2011; Lorrey et al., 2008, 2014; Putnam et al., 2010; Turney et al., 2017), Tasmania (Saunders et al., 2012), southern South America (Aracena et al., 2015; Ariztegui et al., 2010; Lamy et al., 2010; Moreno et al., 2009; Moy et al., 2008; Turney et al., 2015; Waldmann et al., 2010 and others), there are fewer from the subantarctic islands, all of which have a paleovegetation focus (McFadgen and Yaldwyn, 1984; McGlone, 2002; McGlone et al., 2000, 2010; McGlone and Moar, 1997; Turney et al., 2016).

75 Fjords along the eastern side of the subantarctic Auckland Islands of New Zealand (51° 40’S, 166° 10’E) contain sedimentary sequences that have continuously accumulated since the end of the last glacial period, representing a unique opportunity to reconstruct post-glacial SHWW variability in the southwest Pacific. Moreover, the physical properties of the water column and the geochemical nature of fjord sediments and benthic foraminifera are influenced indirectly by the overlying atmospheric circulation via the input of wind-driven precipitation, associated erosion in the catchment, and wind- 80 driven mixing. Here, we use a combination of terrestrial and marine-based proxies from a sediment core recovered from Hanfield Inlet (Figs. 1 and 2) to reconstruct middle to late Holocene SHWW variability and associated changes in shelf hydrography. Drainage basin and fjord circulation responses to variability in the strength and/or position of the SHWW are reconstructed from bulk sedimentary organic carbon isotopes and atomic C/N, which are proxies for organic matter provenance and surface water productivity. In addition, benthic foraminifer stable oxygen and carbon isotopes respond to a 85 combination of bottom water temperature, salinity, productivity, and the input of shelf waters, all of which are driven by the overlying atmospheric circulation.

With the primary goal of improving understanding of subantarctic Holocene SHWW variability, we address the following research questions: 1) What are the modern circulation processes occurring in the Auckland Islands fjords and how is hydrography related to the wind/precipitation regime? 2) What are the departures of foraminiferal calcite from equilibrium 90 isotopic composition and which species are ultimately the most reliable indicators of bottom water conditions in the fjord? 3) Is there multi-proxy evidence for changing fjord circulation and hydrography that can be linked to concomitant changes in atmospheric circulation over the past 5,000 years? Finally, we compare our Auckland Island record of SHWW variability to contemporaneous records from similar latitudes in order to assess symmetry of the westerly wind field since the middle Holocene.



95 2 Study Area

The uninhabited subantarctic Auckland Islands are located on the Campbell Plateau, the mostly submarine southeastern extension of New Zealand's continental landmass (Fig.1), and surficial units are composed almost exclusively of late Cenozoic volcanic rock (Adams, 1983). The western coastline is characterised by steep cliffs that are subject to persistent westerly winds and strong ocean currents. In contrast, the east coast is dominated by sloping ridges, heavily vegetated valleys, inlets and sheltered fjords. The presence of U-shaped valleys, fjords and other glacial landforms (Fleming et al., 1976), combined with radiocarbon-dated peat sequences immediately overlying glacial sediments indicates that the east coast of the Auckland Islands was likely glaciated during Marine Isotope Stage 2 (MIS-2), and that deglaciation was well underway by 15,000 yr BP (McGlone, 2002; McGlone et al., 2000; McGlone and Moar, 1997).

The Auckland Islands are situated at 51° S, within the modern core of the SHWW in the southwest Pacific Ocean (Fig. 1). Like many localities in the southern mid-latitudes, time-averaged zonal SHWW speed is positively correlated with precipitation in the Auckland Islands (Garreaud, 2007), indicating that changes in precipitation through time can be related to past changes in wind strength at this location. At the Auckland Islands, frequent rainfall is combined with persistent cloudiness, gales, and high relative humidity. Meteorological observations since 1991 (Cliflo Database, National Institute for Water and Atmospheric Research) demonstrate little seasonality in rainfall, wind speed and temperature (Fig. S1). Gusts are sourced predominately from the west, exceeding 24 knots for over 300 days of the year, and 33 knots for 200 days of the year (Cliflo Database). East-west aligned fjords act as funnels to channel the prevailing westerlies, and increased wind stress on the water surface can quickly change fjord circulation and hydrography. Hanfield Inlet is isolated from the open ocean by an entrance sill ~12 m deep, and contains two sub-basins that are each ~50 m deep (Fig. 2). Tidal range is <1 m at this location. Sediment cores recovered from basins that are protected from the open ocean or shelf currents by bathymetric sills capture changes in lithogenic input and terrestrial vs marine organic matter (OM_{terr} and OM_{mar} , respectively), which is related to precipitation-driven runoff.

The Auckland Islands are located in the SAZ of the Southern Ocean, with the STF to the north and the SAF to the south. Although the STF southwest of New Zealand shifted rapidly south towards the Auckland Islands during the Last Glacial Maximum and deglaciation in response to an intensification/southward shift in SHWW, the position of this front has remained relatively stable over the Holocene (Bostock et al., 2015), likely due to topographic steering at the 500 m depth contour (Smith et al., 2013). Shelf waters surrounding the Auckland Islands are cold, fresh, and nutrient-poor Subantarctic Surface Water (SASW), with SAMW at depths >300 m, sourced from mixing and upwelling along fronts associated with the ACC (Carter et al., 2009). Because of the proximity of the Auckland Islands to these upwelling fronts, changes in westerly-wind driven upwelling will affect the physical and chemical properties of shelf waters entering Auckland Islands fjords that can potentially be recorded by benthic foraminifera. For example, we anticipate that an increase in Ekman-driven upwelling of fresh and nutrient-rich water along the SAF, associated with positive SAM will decrease surface water $\delta^{18}O$ (decreased salinity) and will decrease $\delta^{13}C_{DIC}$ (increased nutrient content).



3 Methods

3.1 Field Methods

130 In order to 1) characterise the modern fjord environment, and 2) reconstruct past changes from sediment cores, we collected hydrographic data (conductivity, temperature, depth - CTD) and high-resolution sub-bottom seismic profiles, water samples, surface sediment samples, short box cores, and 6 m long piston cores in Hanfield, Norman, Deep, and McLennan Inlets on the eastern margin of the Auckland Islands in February, 2014 (cruise 14PL001) and 2015 (15PL001), using the University of Otago R/V *Polaris II* (Table 1; Figs. 1 and 2). Coring sites were selected by identifying locations with two independent sub-
135 bottom seismic profiling systems: a 24-channel hydrophone system with a boomer source (containing frequencies of 100 to 1000 Hz; penetration depth of 200 m below the sea floor) in tandem with a higher resolution CHIRP system (containing frequencies of 2-10 kHz; 40 m penetration depth below sea floor). The images reveal packages of stratified sediment >10 m thick, free of sediment gravity flows (Fig. 2). The basin immediately landward of the entrance sill in Hanfield Inlet is interpreted to contain two distinctive layers of sediment 4-6 m and ~2 m thick, respectively, separated by a prominent
140 seismic reflector. A transition to units with higher seismic velocity occurs beneath the shallow sedimentary layers. A 5.7 m-long piston core (36P4), recovered from 44 m water depth in Hanfield Inlet was sub-sampled for bulk organic stable isotopes ($\delta^{13}\text{C}$ and $\delta^{15}\text{N}$), total organic carbon (% TOC), total inorganic carbon (% TIC) and total nitrogen (% TN), and benthic foraminifer stable isotopes ($\delta^{13}\text{C}$ and $\delta^{18}\text{O}$). An additional 5.5 m-long piston core (39P4), recovered from 52 m water depth in Hanfield Inlet was examined for sedimentological changes. A short (0-10 cm) box-core containing the sediment-water
145 interface from Hanfield Inlet (36B2) and grab samples from Norman (35G1) and Hanfield (36G1 and 39G1) Inlets, with accompanying CTD data were sampled for foraminifer stable isotope analysis ($\delta^{13}\text{C}$ and $\delta^{18}\text{O}$), in order to assess the isotopic departure of foraminiferal calcite from bottom water equilibrium. In addition, 36B2 was sub-sampled every cm for 10 cm and each interval stained with Rose Bengal solution (2 gL^{-1} in ethanol) in order to assess the depth habitat of benthic foraminifera species. Foraminifer tests that are pink (more than 50% of the test) are regarded to be living, or recently dead at
150 the time of collection.

A series of water column samples from fjords and the continental shelf were collected and filtered, and both water and particulates were analysed for stable isotopes ($\delta^{13}\text{C}_{\text{DIC}}/\delta^{18}\text{O}$ and $\delta^{13}\text{C}/\delta^{15}\text{N}$ respectively). Fjord waters were collected in 10 L Niskin bottles and transferred to 60 mL glass serum bottles for $\delta^{13}\text{C}$ of dissolved inorganic carbon ($\delta^{13}\text{C}_{\text{DIC}}$) and 30 mL glass serum bottles for $\delta^{18}\text{O}$. Samples for $\delta^{13}\text{C}_{\text{DIC}}$ were immediately poisoned with a supersaturated HgCl_2 solution to stop
155 biological activity. Water was also collected in 5 L bottles for particulate organic carbon and nitrogen concentrations and stable isotope composition. These samples were filtered onboard through pre-combusted Whatman GF/C glass fiber filters using a vacuum pump manifold, acidified with 10 % hydrochloric acid to remove any carbonate phases, and oven-dried at 40°C.



3.2 Laboratory Methods

160 3.2.1 Water Column Stable Isotopes

Seawater samples collected in 2014 were analysed for oxygen isotopes and using a Picarro 2120 wave-length-scanned cavity ring-down spectrometer (WS-CRDS), in the Isotrace Laboratory at the University of Otago and average standard deviation for 11 duplicate measurements (fjord, lake, and stream samples) was 0.027 ‰ for $\delta^{18}\text{O}$. The stable isotopic composition of dissolved inorganic carbon ($\delta^{13}\text{C}_{\text{DIC}}$) in 2014 samples, and $\delta^{18}\text{O}$ for the 2015 samples were measured using a Thermo Delta
165 Plus Advantage isotope ratio mass spectrometer (IRMS) interfaced to a Gasbench II via a GC PAL autosampler at the Isotrace Laboratory at the University of Otago. The average standard deviation for 11 duplicates (fjord, lake, and stream samples) was 0.106 ‰ for $\delta^{13}\text{C}_{\text{DIC}}$ and 0.022 ‰ for $\delta^{18}\text{O}$ (11 duplicates; all fjord samples). Stable nitrogen and carbon isotopes of filtered particulates collected in 2014 were measured using a Carlo Erba NC2500 Elemental Analyser, coupled with a Europa Scientific continuous-flow Isotope Ratio Mass Spectrometer (IRMS) using USGS-40 and USGS-41 standards,
170 in the Isotrace Laboratory at the University of Otago. Average standard deviation for USGS-40 was 0.1 ‰ for $\delta^{15}\text{N}$ and 0.042 ‰ for $\delta^{13}\text{C}$, and for USGS-41 was 0.2 ‰ for $\delta^{15}\text{N}$ and 0.049 ‰ for $\delta^{13}\text{C}$. Average standard deviation for duplicate filtered particulates was 1.8 ‰ for $\delta^{15}\text{N}$ (n=4) and 0.25 ‰ for $\delta^{13}\text{C}$ (n=7). Average standard deviation for duplicate bulk sediment was 0.22 ‰ for $\delta^{15}\text{N}$ (n=9) and 0.06 ‰ for $\delta^{13}\text{C}$ (n=9). Stable nitrogen and carbon isotopes of filtered particulates
175 collected in 2015 were measured using a Carlo Erba NA1500 Series 2 Elemental Analyzer coupled to Thermo Finnigan Delta Plus via a ConFlo II open split interface at the Stanford University Stable Isotope Lab (SIBL). Average standard deviation for duplicate filtered particulate samples was 0.35 ‰ for $\delta^{15}\text{N}$ and 0.24 ‰ for $\delta^{13}\text{C}$ (n=2 pairs). Average standard deviation for USGS-40 was 0.13 ‰ for $\delta^{15}\text{N}$ and 0.09 ‰ for $\delta^{13}\text{C}$ (n=27).

3.2.2 Bulk Organic Stable Isotopes

Surface and downcore sediment samples collected in 2014 were freeze-dried, homogenised, and weighed into tin and silver capsules. Increasing volumes of 6 % sulphurous acid were added to silver capsules to remove carbonate phases. Unacidified
180 samples were weighed into tin capsules for concentrations and isotopes of organic nitrogen (% TN and $\delta^{15}\text{N}$). Both acidified (silver) and unacidified (tin) samples were measured for concentrations and isotopes of organic carbon (% TOC and $\delta^{13}\text{C}$) using a Carlo Erba NC2500 Elemental Analyser, coupled with a Europa Scientific continuous-flow IRMS at the Isotrace laboratory at the University of Otago. Average standard deviation for nine duplicate samples was 0.22 ‰ for $\delta^{15}\text{N}$ and 0.06
185 ‰ for $\delta^{13}\text{C}$. The abundance of biogenic carbonate (% TIC) was estimated by subtracting the organic carbon concentrations (silver capsule) from total carbon concentrations (tin capsules).

3.2.3 Radiocarbon Analyses and Chronology

A chronology for core 36P4 was developed using eight AMS radiocarbon-dated acid-base insoluble terrestrial organic macrofossil fragments derived mostly from the >500 μm size fraction (Table 2; Fig. 3). Samples were analysed at the Center



190 for Accelerator Mass Spectrometry (AMS) at Lawrence Livermore National Laboratory, California, USA. Radiocarbon
ages were calibrated using Calib 7.0.4 (Stuiver and Reimer, 1993) and a Southern Hemisphere atmospheric calibration curve
(SHCal13; Hogg et al., 2013). Two samples collected 90 cm apart near the base of the core returned median probability ages
that were approximately the same age, indicating rapid sediment deposition and/or sediment reworking between 370 and 450
cm. We therefore focus our paleoclimate record on the interval from 0-420 cm (approximately 4,000 years), below which
195 smear slides began to show disaggregated sponge spicules and magnetic susceptibility abruptly increased to the highest
values observed in the core. A Bayesian modelling approach was used to model the distribution of time throughout the core
stratigraphy, and the oldest two ^{14}C dates from the disturbed section were not included in this model. Bacon 2.2 (Blaauw and
Christen 2011) was used, with the following priors: accumulation shape = 1.5, accumulation mean = 10 yrcm^{-1} , memory
mean = 0.7, strength mean = 4 (Z), with a 71.5 cm section. The weighted mean calibrated age BP from the 95 % confidence
200 interval of the Markov Chain Monte Carlo simulations is used. The age model indicates that the core top is around 400 years
old, indicating that the most recent part of the record was not recovered during piston coring.

3.2.4 Benthic Foraminifer Stable Isotopes

Benthic foraminifera *Cibicides* spp., *Nonionellina flemingi*, *Trifarina angulosa*, and *Bulimina marginata* f. *marginata* were
picked from the 125-250 μm fraction, and *Quinqueloculina seminula* from the <250 μm fraction, and were cleaned by briefly
205 sonicating in distilled water. Foraminifer $\delta^{13}\text{C}$ and $\delta^{18}\text{O}$ were measured using a Kiel IV carbonate device, coupled to a
MAT-253 Mass Spectrometer at the National Institute of Water and Atmospheric Research (NIWA) in Wellington, New
Zealand. Internal precision of the instrument was monitored by measuring NBS-19 with each set of unknown samples and
standard deviation for NBS-19 was 0.01-0.03 ‰ for $\delta^{13}\text{C}$ and 0.02-0.07 ‰ for $\delta^{18}\text{O}$. The standard deviation of one replicate
sample for *Cibicides* spp. (from 36P4) is 0.1 ‰ for both $\delta^{13}\text{C}$ and $\delta^{18}\text{O}$. The average standard deviation of replicate samples
210 for *N. flemingi* (from 36P4) was 0.27 ‰ for $\delta^{13}\text{C}$ (n=3) and 0.07 ‰ for $\delta^{18}\text{O}$ (n=4).

3.2.5 Calculating Vital Offset of Benthic Foraminifer $\delta^{18}\text{O}$ from Equilibrium

Modern bottom water $\delta^{13}\text{C}_{\text{DIC}}$, $\delta^{18}\text{O}$ ($\delta^{18}\text{O}_w$) and temperature were measured at Site 35 (Norman Inlet; CTD_001), and Sites
36 and 39 (Hanfield Inlet CTD_002 and CTD_004, Table S1). Expected foraminifer oxygen isotopic composition
precipitated in equilibrium with bottom water ($\delta^{18}\text{O}_c$) for a given temperature (T) was calculated for each site using Eq.(1), a
215 linear paleotemperature equation derived by Marchitto et al., 2014 (Table 2). Equation 1 is indistinguishable from that of
Kim and O'Neil (1997), derived from experiments involving precipitation of inorganic calcite in seawater at different
temperatures hence is here considered appropriate for species other than *Cibicides*.

$$(\delta^{18}\text{O}_c - \delta^{18}\text{O}_w(\text{VSMOW}) + 0.27) = -0.225T + 3.50 \quad (1)$$

220 **Equation 1.** Where $\delta^{18}\text{O}_c$ is average oxygen isotopic composition of calcite precipitated in equilibrium with bottom water $\delta^{18}\text{O}$,
 $\delta^{18}\text{O}_w$ is measured bottom water oxygen isotopic composition (relative to VSMOW), and T is bottom water temperature in $^{\circ}\text{C}$
(Marchitto et al., 2014). A correction factor of 0.27 ‰ is applied when converting $\delta^{18}\text{O}$ from the VSMOW to VPDB scale (Hut,
1987).



4 Results

4.1 Modern Fjord Hydrography and Water Column Stable Isotopes

225 CTD profiles and water isotopes measured landward of submarine sills during the 2014 and 2015 field seasons reveal that the fjords are only stratified for very short intervals of time (Fig. 4). During 1-2 day intervals when dry conditions and low wind velocities persist, surface water temperature (upper ~4 m) and $\delta^{18}\text{O}$ (upper ~10 m) are elevated, and salinity is slightly depressed (upper ~4 m). During intervals when precipitation and high wind velocities persist, temperature and salinity show little variation with depth. Particulate $\delta^{13}\text{C}$ and $\delta^{15}\text{N}$ are somewhat more positive (+ ~1 ‰) during rainy and high wind
230 synoptic conditions compared to times when dry / low wind velocities persist, although there is no significant difference in the vertical isotopic gradient in either regime. Atomic C/N of particulate organic matter (OM) does not vary throughout the water column during rainy / high wind conditions, but appears to be elevated in the subsurface during dry / low wind conditions.

Physical properties and water isotopes measured in 2014 on the continental shelf between Hanfield and Norman Inlet
235 demonstrate little variation in temperature, salinity, $\delta^{18}\text{O}$, and particulate $\delta^{15}\text{N}$ and $\delta^{13}\text{C}$ with depth (Table S1). Average salinity outside of the fjords is 34.5, temperature is 10.5° C, $\delta^{18}\text{O}$ is -0.14 ‰ and $\delta^{13}\text{C}_{\text{DIC}}$ is 0.15 ‰. Fjord salinity during sunny and dry conditions is similar to outside of the fjord, but is depressed by ~0.25 during rainy and high wind synoptic conditions (Fig. 3).

Filtered particulate samples are separated into five groups based on C and N isotopic composition: low salinity layer
240 (particulate OM samples from depths <10 m in Hanfield and Norman Inlets), deep fjord (particulate OM samples from depths >10 m in Hanfield and Norman Inlets) offshore (particulate OM samples from the continental shelf seaward of the sill), lake samples (particulate OM samples from 3 lakes on the main island), and fjord sediment samples surface sediment samples from Hanfield Inlet (Fig. S2). There is no obvious difference between fjord surface water and deep water fjord stable isotopic ratio and atomic C/N. The $\delta^{13}\text{C}$ of fjord particulate OM samples generally exhibits more positive values than
245 the shelf surface waters, although CTD_003 taken from outside Norman and Hanfield Inlets has a more positive average $\delta^{13}\text{C}$ composition (-21.52 ‰) and lower average C/N (5.51) relative to Hanfield Inlet during dry and low wind conditions (-23.1 ‰ and 7.17, respectively). Samples collected farther offshore from Chambres Inlet and near Stewart Island in 2014 have $\delta^{13}\text{C}$ values that average -22.01 ‰. Sediment samples from Hanfield Inlet exhibit an intermediate $\delta^{13}\text{C}$ value and C/N is elevated by ~2-3 relative to particulate OM samples. There are no obvious patterns in $\delta^{15}\text{N}$ across different sample groups.

250 4.2 Modern Benthic Foraminifer Stable Isotopes

Averaged $\delta^{18}\text{O}_{\text{foram}}$ for selected species of benthic foraminifera from grab and box-core samples in both Norman and Hanfield Inlets are compared to $\delta^{18}\text{O}_{\text{c}}$, calculated from measured $\delta^{18}\text{O}_{\text{w}}$ and temperature during the summers of 2014 and 2015 (Tables 2 and 3, Fig. 5). Epifaunal *Cibicides* spp. (n=3) precipitates $\delta^{18}\text{O}$ within the range of expected $\delta^{18}\text{O}_{\text{c}}$, hence in equilibrium with bottom water. Shallow infaunal New Zealand endemic *N. flemingi* (n=5) is enriched in ^{18}O relative to what



255 is predicted for equilibrium fractionation. Other species including *B. marginata* f. *marginata* (n=5), *T. angulosa* (n=6) and *Q. seminula* (n=6) also show positive offsets relative to $\delta^{18}\text{O}_c$, and the degree of offset generally increases with increased depth habitat. Rose Bengal staining of box-core samples indicates that *B. marginata* f. *marginata* and *C. lobatulus* live at 0-1 cm depth, *N. flemingi*, *Sigmoilopsis elliptica* and *Anomalinoidea sphericus* at 1-2 cm, *Cassidulina carinata* at 2-3 cm and *Bolivina* cf. *earlandi* at 3-4 cm. Although *T. angulosa* was not found in this study, it is known to be shallow infaunal, and
260 lives at 0-1cm depth (Mackensen et al., 1990). *Q. seminula* was likewise unstained, so the depth habitat in Hanfield remains unconstrained. However, Scott et al., (2001) indicate that this species is shallow infaunal or possibly epifaunal.

4.3 Sedimentology, Magnetic Susceptibility, and Bulk Organic Carbon and Nitrogen Isotopes

Sediment core 36P4 is composed of homogenous dark brown fine-grained sand and mud, faecal pellets, small (<500 μm) benthic and planktonic foraminifera, gastropods, ostracods, calcareous nannofossils, diatoms and terrestrial plant debris. The
265 upper ~90 cm of the core is slightly bioturbated and there are no significant lithological distinctions (colour, grain size, sediment type) downcore. Sediment core 39P4 contains a sharp transition from brown foraminifer-bearing fine-grained sand and mud to dark freshwater diatom-bearing clays.

Magnetic susceptibility (MS), wt % TN, TOC and TIC, bulk organic $\delta^{13}\text{C}$ and $\delta^{15}\text{N}$, and atomic C/N for core 36P4 are plotted against depth in Fig. 6 and age in Fig. 7. The core is subdivided into three sections based on prominent shifts in
270 multiple proxies (Fig. 7). From ~4,800-4,000 yr BP, MS is highly variable, wt% TN, TOC and TIC is relatively low. From ~4,000-1,600 yr BP, MS, wt % TN, TOC and TIC and bulk organic $\delta^{13}\text{C}$ and C/N remain relatively unchanged. From ~1,600-900 yr BP, wt % TN and TOC increases, bulk organic $\delta^{13}\text{C}$ is more positive, $\delta^{15}\text{N}$ is more negative, and atomic C/N becomes lower. From 900-500 yr BP, wt % TN and TOC increases while MS decreases, and bulk organic $\delta^{13}\text{C}$ is more positive while C/N remains unchanged.

275 4.4 Downcore Benthic Foraminifer Stable Isotopes

Downcore isotope results for *Cibicides* spp. and *N. flemingi* are shown in Table S2, Fig. 8, and Fig. S3, with no correction for species-specific vital offsets. Both isotopes of epifaunal *Cibicides* spp. exhibit similar trends downcore, with more negative $\delta^{13}\text{C}$ values corresponding to more negative $\delta^{18}\text{O}$ (Fig. S3). The range of variability in both isotopes increases above
280 100 cm depth (~1,600 yr BP). The overall trend and range of $\delta^{18}\text{O}$ for both species is similar, whereas the trend and range for $\delta^{13}\text{C}$ differs between each species (Fig. 8). *N. flemingi* exhibits more negative $\delta^{13}\text{C}$ values (downcore range from ~-0.5 to -3.5 ‰) whereas *Cibicides* spp. demonstrates more positive $\delta^{13}\text{C}$ values (downcore range from ~0 to -1.5 ‰).



5 Discussion

5.1 Modern Fjord Circulation and Response to SHWW Variability

In order to reconstruct past changes in atmospheric circulation at the Auckland Islands, modern process studies are required to understand how westerly winds and associated precipitation modifies fjord circulation, influences the delivery of OM from both terrestrial (OM_{terr}) and marine (OM_{mar}) sources, and alters the physical and chemical nature of the water column. In temperate fjords, particularly in Fiordland (~500 km to the north of the Auckland Islands), increased precipitation delivers freshwater with abundant terrestrial organic matter to the head and margins of fjords, promoting the formation of a buoyant, seaward-flowing low salinity surface layer enriched in OM_{terr} , which is replaced by return flow from the open ocean of saline water enriched in OM_{mar} (Hinojosa et al., 2014; Knudson et al., 2011; Pickrill, 1987; Stanton, 1984). In these settings, the thickness and extent of the low salinity layer primarily depends upon precipitation amount, the size of the catchment relative to the volume of the fjord, the nature of the fluvial drainage network discharging at the head and other locations within the fjord, and wind-induced mixing (Gibbs et al., 2000). Return flow of ocean water is limited by sill height and mixing processes with the overlying low salinity layer (Pickrill, 1987; Stanton, 1984).

CTD data collected from Hanfield and Norman Inlets in 2014 and 2015 indicate the absence of a significant low salinity layer or any persistent stratification of the water column (Fig. 4). Our limited summer observations indicate that although the upper ~4 m of the water column can thermally stratify by 0.7° C, the water column quickly becomes isothermal once the next frontal system passes over the islands. Moreover, small catchment/fjord areas result in limited fluvial discharge at the head of the fjord which prevents formation of a significant low salinity layer. We speculate that strong winds that flow parallel to the fjord axis mix the water column and further prevent the establishment of significant estuarine circulation.

The isotopic composition and atomic C/N of particulate OM can be used to determine sediment provenance in continental margin settings, and when measured downcore in fjord sediment cores, these parameters can be used as a potential proxy for OM_{terr} delivery derived from westerly precipitation (Hinojosa et al., 2014; Knudson et al., 2011; Meyers and Terranes, 2001; Walinsky et al., 2009). OM_{terr} is characterised by more negative $\delta^{13}C$ and $\delta^{15}N$ whereas OM_{mar} is characterised by more positive $\delta^{13}C$ and $\delta^{15}N$, although it is important to note that bulk sediment organic matter can also be influenced by surface water productivity in a stratified water column and potentially by post-depositional degradation by bacteria (Meyers and Terranes, 2002). Similarly, atomic C/N can be helpful to discriminate between terrestrial and marine OM sources. Terrestrial vascular plants are cellulose-rich and contain a relatively high proportion of carbon compared to marine algae which are protein-rich and contain more nitrogen (Meyers and Terranes, 2002). A higher C/N ratio therefore is indicative of a larger contribution of OM_{terr} , relative to OM_{mar} and vice versa.

Hanfield Inlet demonstrates a distinct hydrographic response to changes in SHWW-derived precipitation and mixing (Fig. 4). During intervals when prevailing wind speeds and precipitation is low, the fjord is weakly stratified due to solar heating (elevated temperature) and evaporation (enriched $\delta^{18}O$ / increased salinity) in the uppermost part of the water column. During periods with high winds and rainfall, any weak stratification rapidly breaks down, and there is no vertical change in



315 temperature, salinity, and C/N, likely due to wind-induced mixing and subsequent overturning of the water column. Also during periods of high winds and precipitation, water column salinity is slightly depressed, relative to periods of low winds and precipitation. We do not observe a reduction in fjord bottom water $\delta^{18}\text{O}$ during rainy/high wind conditions, but this is likely due to our inability to sample the water column across a range of seasons/years. We speculate that sustained enhanced freshwater input into the fjord and wind-induced mixing of the water column does reduce the $\delta^{18}\text{O}$ of bottom water.

320 Enhanced rain is also expected to increase erosion and delivery of lithogenic material into the fjord basin, although this is not assessed in this study.

Bulk sedimentary stable isotopes and C/N ratios provide further insight into the hydrographic response of fjords to increased westerly wind-derived precipitation (Fig. 4; Fig. S2; Table S1). In contrast to fjords in Fiordland, southern New Zealand, Auckland Islands particulate data indicate a greater contribution of OM_{mar} (more positive $\delta^{13}\text{C}$ and lower C/N during periods

325 of sustained high winds, suggesting that an increased delivery of OM_{mar} through entrainment in the return flow of shelf waters overwhelms the signal of increased freshwater input from runoff (with entrained OM_{terr}). Because the Auckland Islands fjords are shallower and shorter, have much smaller catchment areas and experience lower precipitation than those of southern New Zealand, a significant low salinity surface layer is not created. Nevertheless, because bulk sedimentary $\delta^{13}\text{C}$ is more positive and C/N is lower during windy periods relative to low wind conditions, these parameters can be used as

330 indirect proxies for wind strength at the Auckland Islands. Because bulk sedimentary $\delta^{15}\text{N}$, which can be influenced by additional processes such as denitrification and substrate evolution (Altabet and Francois, 1994; Meyers and Teranes, 2001), shows no discernible difference in isotopic composition between water masses inside and outside of the fjord (Fig. S2), it is not incorporated into our paleoclimate discussion.

In summary, our observations indicate that an increase in wind strength and associated precipitation at the Auckland Islands

335 induces complete mixing of the fjord water column, reduces salinity, and increases the contribution of OM_{mar} . We speculate that increased wind strength induces complete mixing of fjord waters, and that wind stress aligned parallel to the axis of east-west orientated fjords increases the outflow of surface waters, driving return flow of OM_{mar} -dominated shelf waters. Further hydrographic studies of Auckland Island fjords during different seasons would be required to vigorously test this hypothesis, however given present information and our hypothesised link between westerly wind-driven precipitation and delivery of

340 OM into the fjord, downcore changes in bulk sedimentary $\delta^{13}\text{C}$ and C/N are interpreted here as indirect proxies for wind strength, with more positive $\delta^{13}\text{C}$ and a lower C/N indicative of high winds and associated precipitation.

5.2 Modern Benthic Foraminifer Oxygen Isotopes

Epifaunal *Cibicides* spp. recovered from box-core and grab samples in Hanfield Inlet precipitates within the range of calculated $\delta^{18}\text{O}_c$ for the entire range of temperatures (9.9-10.55 °C) and $\delta^{18}\text{O}_w$ (-0.26 to 0.31‰) measured in Hanfield and

345 Norman Inlets (Fig. 5). Previous studies have also demonstrated that *Cibicides* spp. precipitates in equilibrium with ambient bottom waters (Graham et al., 1981; Grossman, 1984; Hald and Vorren, 1987; Lynch-Stieglitz et al., 1999; Marchitto et al., 2014; McCorkle et al., 1997). New Zealand endemic and infaunal *N. flemingi* also recovered in box-core and grab samples



from Hanfield and Norman Inlets exhibits isotopic values that are more positive relative to $\delta^{18}\text{O}_c$, similar to the Northern Hemisphere species *N. laboradorica* (Grossman, 1984).

350

5.3 Middle to Late Holocene SHWW Variability

Geophysical and sedimentological data from Hanfield Inlet reveal the deglacial and post-glacial history of Hanfield Inlet. A transition in core 39P4 (collected 0.5 km to the east of 36P4; Figs 1 and 2) is characterised by an abrupt change from dark, organic-rich mud with freshwater diatoms to foraminifer-bearing fine-grained sand and mud, indicating that the fjord once contained a lake landward of the entrance sill. Two sharp transitions identified in seismic profiles occur beneath the fine grained marine and lacustrine sedimentary package and probably represent glacial sediment deposited on eroded volcanic basement during glacial retreat. Based on the height of the submarine sill (~12 m) and relative sea level curves from southern New Zealand (Clement et al., 2016; Dlabola et al., 2015), marine incursion of Hanfield Inlet likely occurred between 10,000 and 9,000 yr BP.

360 Sedimentological evidence for disturbance and radiocarbon results from 36P4 indicate that the bottom part of the core (370-450 cm) contains reworked sediment, probably the result of a single localised slump event. For this reason, the oldest ^{14}C date incorporated into the Bayesian age model for 36P4 was that at 366 cm (4691 ± 30 yr BP), and only the undisturbed section of the core is used for SHWW reconstruction.

Fjord conditions are relatively stable from ~4,000 to 1,600 yr BP, as indicated by the generally unchanging wt % of TN, TOC and TIC, and bulk organic $\delta^{13}\text{C}$ and atomic C/N (Figs. 6 and 7). This entire interval is characterised by more negative bulk sedimentary $\delta^{13}\text{C}$ and elevated atomic C/N, compared to the uppermost part of the core <1,600 yr BP (Fig. 6), indicating a smaller contribution of OM_{mar} and therefore an overall increased stratification and decreased SHWW strength during this interval.

Concomitant shifts in MS and bulk sedimentary data at ~1,600 yr BP and ~900 yr BP indicate increased variability in fjord hydrography related to changes in atmospheric circulation during the late Holocene (Figs. 6 and 7). From 1,600-900 yr BP, increased wt % TN, more positive bulk organic sedimentary $\delta^{13}\text{C}$ and lower C/N indicates an increased contribution of OM_{mar} to the fjord, suggesting invigorated wind-driven mixing and return flow of shelf waters. In addition, increased MS during this interval during which non-lithogenic sedimentary components (wt % TN, TOC and TIC) remain stable indicates increased supply of lithogenic material via runoff, corroborating the interpretation of this period as an interval of high winds/precipitation. From 900-500 yr BP, a decrease in MS is accompanied by an increase in % TN and TOC, which could represent dilution of lithogenic material as well as reduced lithogenic input (Figs. 6 and 7). Increased % TN and TOC at this time probably represents increased surface water productivity (rather than an increase in precipitation and wind strength), which is reflected by more positive $\delta^{13}\text{C}$. Increased fjord water productivity could be related to increased stratification under weakened winds or input of nutrient-rich waters from outside of the fjord. From 1,600-500 yr BP, bulk sedimentary $\delta^{13}\text{C}$ and



380 $\delta^{15}\text{N}$ become decoupled (Fig. 6), but because $\delta^{15}\text{N}$ in the modern fjord system is unrelated to the source of organic matter (Fig. S2), it is not considered a suitable proxy to interpret changes in westerly wind-driven precipitation in Hanfield Inlet. Superimposed on long-term paleoenvironmental and paleoclimate changes are sub-millennial scale variations in fjord bottom water chemistry, as indicated by paired changes in benthic foraminifer stable isotopes (Figs. 7 and 8). Covariance of both $\delta^{18}\text{O}$ and $\delta^{13}\text{C}$ for epifaunal *Cibicides* spp. (Fig. S3) indicates that fjord hydrography is influenced by the introduction of

385 shelf waters with different physical properties and an isotopically distinct composition (our limited observations indicate that shelf water $\delta^{18}\text{O}$ and $\delta^{13}\text{C}_{\text{DIC}}$ are characterised by more negative values than fjord waters; Supp. Table 1). $\delta^{18}\text{O}$ of infaunal species *N. flemingi* covaries with *Cibicides* spp. $\delta^{18}\text{O}$, while *N. flemingi* $\delta^{13}\text{C}$ differs, reflecting the porewater $\delta^{13}\text{C}_{\text{DIC}}$ influence often observed in infaunal $\delta^{13}\text{C}$ (Mackensen et al., 2000; McCorkle et al., 1990), rather than ambient bottom water conditions. Overall, covariance between infaunal and epifaunal $\delta^{18}\text{O}$ and disparity in $\delta^{13}\text{C}$ indicates that there is no

390 significant post-depositional overgrowth in Hanfield Inlet benthic foraminifera (Fig. S3). The oxygen isotopic composition of benthic foraminifera is dependent on temperature, salinity, species-specific offsets, and the isotopic composition of the source water (Ravelo and Hillaire-Marcel, 2007). Sub-millennial changes in the $\delta^{18}\text{O}$ downcore stratigraphy are as large as 1.0‰ (Figs. 7 and 8), which would correspond to fjord bottom water temperature changes greater than 4°C (~+0.23‰ per 1°C increase; Marchitto et al., 2014). This is unlikely given regional terrestrial temperature reconstructions (McGlone et al.,

395 2010), and the <0.5 ‰ range of Holocene $\delta^{18}\text{O}$ variability in planktic foraminifera derived from a transect of sediment cores collected in the Solander Trough close to the Auckland Islands (Bostock et al., 2015). Therefore, a combination of local salinity effects, temperature changes, and the $\delta^{18}\text{O}$ of regional waters likely influence the $\delta^{18}\text{O}$ of benthic foraminifera in Hanfield Inlet. Measured summer salinity profiles indicate a range in salinity from 34.5 to 34, which corresponds to a 0.2 ‰ decrease in $\delta^{18}\text{O}_c$ (Lynch-Stieglitz et al., 1999), although given our limited measurements (two field seasons), the fjord

400 salinity minimum could be lower during sustained input and mixing of westerly wind-derived fresh water into the fjords. Based on our observations, we interpret more negative benthic foraminifer $\delta^{18}\text{O}$ to reflect enhanced westerlies, which increases the input and mixing of more negative $\delta^{18}\text{O}$ freshwater into the fjords, prohibits long-term stratification of the fjord, and allows for the introduction of more southerly sourced Southern Ocean water (with a stable isotopic composition of ~ -0.5 ‰; Boyer et al., 2013), sourced from northwards export of waters upwelled along the SAF. Alternatively, increased

405 SST, which is shown in data reanalysis studies to be related to a positive phase of the SAM, associated with increased westerly strength over this part of New Zealand (Ummenhofer et al., 2009; Ummenhofer and England, 2007) would cause a decrease in surface water $\delta^{18}\text{O}$.

Benthic foraminifer $\delta^{13}\text{C}$ reflects ambient bottom water $\delta^{13}\text{C}_{\text{DIC}}$, which is controlled by air-sea exchange of CO_2 , biological processes of photosynthesis and respiration, and addition of water masses with signature isotopic characteristics (Ravelo and

410 Hillaire-Marcel, 2007). Increased input of freshwater during periods of intensified winds and rainfall would decrease $\delta^{13}\text{C}_{\text{DIC}}$ because of increased respiration and remineralisation of ^{12}C -rich OM_{terr} , which is consistent with our interpretation of decreased $\delta^{18}\text{O}$ also being indicative of increased wind strength. In addition, fjord water $\delta^{13}\text{C}_{\text{DIC}}$ is most likely to be influenced by water masses entering from outside of the fjord. In the SAZ of the Southern Ocean, models based on satellite



data (Lovenduski and Gruber 2005) demonstrate positive SST anomalies (manifested as more negative foraminifer $\delta^{18}\text{O}$ in
415 the current record) and lower surface water productivity (inferred by low chlorophyll concentrations), associated with a
positive SAM and intensified SHWW. Increased water column stratification because of elevated SST is hypothesised to
reduce productivity, by limiting macronutrient supply to the euphotic zone (Lovenduski and Gruber, 2005), which will cause
 $\delta^{13}\text{C}_{\text{DIC}}$ to be more negative because less of the light isotope, ^{12}C can be preferentially utilised by macro nutrient-limited
phytoplankton. In addition, other modelling studies have shown that the recent southward shift in the SHWW has increased
420 upwelling and northward advection of SAMW at $\sim 60^\circ\text{S}$ (Wetzel et al. 2005; Le Quéré et al. 2007; Lovenduski et al. 2008).
Northward export of SAMW with more negative $\delta^{13}\text{C}_{\text{DIC}}$ (contains more ^{12}C , released by remineralisation of organic matter
at depth) could also contribute to lowering of SAZ surface water $\delta^{13}\text{C}_{\text{DIC}}$. Taken together, these results suggest that variations
in the $\delta^{18}\text{O}$ and $\delta^{13}\text{C}$ of benthic foraminifera recorded in Hanfield Inlet are controlled indirectly through the influence of the
strength and latitudinal position of the SHWW on shelf/fjord hydrography during the middle to late Holocene. The
425 foraminifer isotope record from Hanfield Inlet exhibits more negative $\delta^{18}\text{O}$ (decreased salinity from local rainfall and fjord
mixing and an increased influence of a southerly-sourced water masses), and more negative $\delta^{13}\text{C}_{\text{DIC}}$ (increased Ekman
upwelling and northward export of SAMW), interpreted here to be the result of strengthened SHWW in the southwest
Pacific Ocean. This interpretation is consistent with modelled increased SST and decreased surface water productivity in the
SAZ under positive SAM (Lovenduski and Gruber, 2005), although it is important to note that extra-topical variability
430 driven by ENSO also affects SSTs around New Zealand (Ummenhofer et al., 2009). In addition, increased wind-driven
upwelling and northward export of SAMW with depleted $\delta^{13}\text{C}_{\text{DIC}}$ (Lovenduski et al., 2008; Le Quéré et al., 2007; Wetzel et
al., 2005) could contribute to lowering $\delta^{13}\text{C}_{\text{DIC}}$ at the mid-latitudes.

Our middle to late Holocene paleoclimate reconstruction at the Auckland Islands, using both terrestrial and marine proxies
indicates increased influence of the SHWW during the late Holocene. Around 1,600 yr BP, bulk sedimentary $\delta^{13}\text{C}$ becomes
435 more positive and atomic C/N decrease, indicating an increased contribution of OM_{mar} as a result of wind-induced mixing
and enhanced return flow of shelf waters. Increased variability in benthic foraminifer $\delta^{18}\text{O}$ and $\delta^{13}\text{C}$ during the late Holocene
represents enhanced SHWW influence. Paired decreases in benthic foraminifer $\delta^{18}\text{O}$ and $\delta^{13}\text{C}$ are interpreted as increased
input of shelf waters with characteristic water properties and mixing of freshwater into the fjord, both processes which are
related to increased SHWW strength in the southwest Pacific Ocean. From $\sim 900\text{-}500$ yr BP, surface productivity increases,
440 possibly related to increased fjord stratification due to a reduction in westerly wind-derived precipitation, or changes in shelf
water hydrography.

5.4 Comparison to Other Records of SHWW Variability

5.4.1 New Zealand

Previous Holocene SHWW reconstructions at the Auckland and other subantarctic islands are based on palynology from peat
445 cores (McGlone, 2002; McGlone et al., 2000, 2010; McGlone and Moar, 1997) and tree-line reconstructions (Turney et al.,



2016), and are broadly consistent with our interpretations of increased SHWW influence from ~1,600-900 yr BP (Fig. 9). Tree-line reconstructions suggest increased wind strength from 2,000-1,000 yr BP (Turney et al., 2016), and the establishment of tall *Metrosideros* forest from 5,500-4,000 yr BP (McGlone et al., 2000) suggests strengthened SHWW and decreased cloudiness over the middle and late Holocene. Wide-spread die back of *Metrosideros* forest and replacement by
450 woody shrubs and trees such as *Dracophyllum*, *Myrsine*, and *Raukaua* in a bog core after 1,500 yr BP indicates higher water tables and increased exposure (McGlone et al., 2000). McGlone et al. (2000) also demonstrate several millennial-scale expansions and collapses of *Metrosideros* forest since 4,000 yr BP, similar to millennial-scale fluctuations in SHWW variability which is manifested in our foraminifer isotope record of shelf water hydrography.

A comparison of SHWW records from Fiordland (45°S) with the current record (51°S) allows for assessment of potential
455 latitudinal shifts in the wind field over New Zealand. Two intervals of elevated westerly wind-derived precipitation in Fiordland reconstructed using bulk organic stable isotopes as a proxy for OM provenance occurred from 2,000-1,400 yr BP and from 1,100-750 yr BP (Knudson et al., 2011). These two periods broadly overlap with our interpreted strengthening of the winds from downcore $\delta^{13}\text{C}$ and C/N of bulk sediment, and from benthic foraminifer stable isotopes (Fig. 8). Based on this comparison, we interpret that the westerlies were strong over ~6° of latitude within the New Zealand sector of the
460 southwest Pacific Ocean from 1,600-1,400 and 1,100-750 yr BP. Weakened wind strength in Fiordland from 1,400-1,100 yr BP while westerlies were still strong at the Auckland Islands (an anti-phased relationship) argues for a southward shift or contraction in SHWW, rather than a change in intensity at this time. Weakened winds over Fiordland after 750 yr BP at the beginning of the Little Ice Age (LIA; ~700-100 yr BP) is contemporaneous with our interpretation and that of Turney et al.,
465 (2016) of decreased influence of the westerlies at the Auckland Islands from ~1000-900 yr BP. Taken together, these results suggest that the winds were shifted southwards and/or expanded over southern New Zealand prior to the LIA, and began to migrate northwards towards mainland New Zealand a few centuries prior to the LIA.

5.4.2 Southern South America

Select SHWW records from a range of latitudes are compared with the current record in order to assess zonal symmetry during the middle to late Holocene (Fig. 9). A study from a fjord system in the Strait of Magellan (53° S), southern
470 Patagonia, reconstructs Holocene changes in westerly wind-derived precipitation and associated changes in salinity and productivity using accumulation rates of biogenic silica, organic carbon, inorganic carbon (carbonate), and siliciclastics (Aracena et al. 2015). Increased siliciclastic, organic carbon (both marine and terrestrial) and carbonate AR at ~2 ka likely indicates an intensification of freshwater flux from increased precipitation (hence SHWW intensification) at this time. Slightly elevated glacial clay content, increased terrestrial organic carbon AR and a significant decrease in carbonate
475 accumulation rate from 3.2-2.2 ka are inferred to reflect another period of intensified westerlies. An additional $\delta^{18}\text{O}$ record from fine-grained (<63 μm) biogenic carbonate recovered in a sediment core from Lago Guanaco, Chilean Patagonia (51°S) indicates increased wind-driven evaporation from ~1,600 yr BP (Fig. 9; Moy et al., 2008). Both of these records from southern South America indicate roughly contemporaneous intensification of the SHWW at comparable latitudes to our



480 Auckland Islands record, suggesting that the winds behaved in a zonally consistent manner across the Pacific Ocean, or that climate variability in both locations was controlled by a common forcing mechanism, such as atmospheric teleconnections between the low and high latitudes of the Pacific Ocean (Haug et al., 2001; Mayewski et al., 2004; Villalba et al., 1997).

5.4.3 Western Antarctic Peninsula

Upper ocean temperatures along the western Antarctic Peninsula (WAP) are largely modulated by SHWW-driven upwelling of relatively warm (~2°C) CDW onto the continental shelf (Cook et al., 2016; Martinson et al., 2008), hence ocean temperature reconstructions from this area can be interpreted in terms of wind strength (Shevenell et al., 2011). With 485 increased SHWW influence (increased strength/ more southward location), upwelling of CDW increases which warms shelf waters along the WAP. An upper ocean (0-200 m) temperature record derived using the TetraEther indeX of 86 carbon atoms (TEX₈₆) from Palmer Deep (64°S, 64°W; Fig. 9) demonstrates warming around 1,600 yr BP, indicative of increased SHWW influence at this latitude, associated with initiation of atmospheric teleconnections between the WAP and Equatorial 490 Pacific (Shevenell et al., 2011). Initiation of teleconnections from low to high latitudes may also influence wind variability in the southwest Pacific via the influence of ENSO and SAM on atmospheric circulation on extratropical regions of the Southern Hemisphere. For example, SSTs and presumably $\delta^{13}\text{C}_{\text{DIC}}$ in surface water masses around New Zealand are also affected by zonal circulation patterns via anomalous Ekman transport and heat fluxes (Ummenhofer and England, 2007). Modelling studies described above demonstrate that the modern southward shift of the SHWW belt is manifested as 495 increased SST and decreased productivity in the SAZ, therefore this process could be partially controlling surface water $\delta^{18}\text{O}$ and $\delta^{13}\text{C}_{\text{DIC}}$ over the southwest New Zealand continental shelf. Taken together, this correspondence indicates wide-spread changes in physical oceanography related to atmospheric variability over the middle to late Holocene.

In summary, SHWW records from Patagonia (51°S and 53°S) and the WAP (64°S) argue for increased wind strength during the late Holocene (onset between 2,000 and 1,600 yr BP), and new and existing (McGlone et al., 2000; Turney et al., 2016) 500 evidence from the Auckland Islands demonstrates a broadly contemporaneous increase in wind strength, supporting the argument that the SHWW have behaved in a zonally consistent manner from at least 1,600-900 yr BP. However, before 2,000 yr BP, antiphased relationships in wind strength at comparable latitudes including the current record, implies asymmetry in the SHWW during the middle Holocene (Fletcher and Moreno, 2012). However, it should be noted that interpretations of SHWW variability are complicated due to varying sensitivity of different proxies, and the contradictory 505 nature of using multiple proxies with poorly defined relationships to the modern environment (see discussions by Kilian and Lamy, 2012 and Fletcher and Moreno, 2012).

5.5 Assessment of SHWW symmetry during the LIA

The current multiproxy westerly wind reconstruction from Hanfield Inlet, and tree-stump reconstructions (Turney et al., 2016) indicate weakened westerly winds over the Auckland Islands from 1,000-900 yr BP, while winds remained strong 510 over Fiordland, Southern New Zealand, until weakening at 750 yr BP (Knudson et al., 2011). Taken together, these results



indicate a northward shift or contraction of the SHWW over New Zealand from 900-750 yr BP, roughly coincident with the beginning of the LIA, which is a period of cool summer temperatures (anomaly of $-0.56 \text{ }^{\circ}\text{C} \pm 0.29 \text{ }^{\circ}\text{C}$; Cook et al., 2002; Lorrey et al., 2014) and glacial advance in southern New Zealand (Lorrey et al., 2014; Putnam et al., 2010). Decreased wind strength recorded in Fiordland after 750 kyr that coincides with glacier advance in the Southern Alps can be reconciled if
515 cooler summer temperatures are dominating glacier mass balance over precipitation associated with the SHWW. In addition, data reanalysis of precipitation patterns in Fiordland and the Southern Alps demonstrate that these areas are affected to different degrees by variations in the SAM and ENSO, also explaining regional differences in these records during the LIA (Ummenhofer et al., 2009).

Reconstructions of the SAM using south Pacific tree-ring records (Villalba et al., 1997, 2012) and the James Ross Island ice
520 core (eastern Antarctic Peninsula; Abram et al., 2014) indicate a predominately negative phase of the SAM during the LIA. Some records from Antarctica also document the LIA, which is manifested as cool conditions in the Ross Sea (Bertler et al., 2011; Rhodes et al., 2012), and at Siple Dome (Mosley-Thompson et al., 1990), and periods of glacial advance along the western Antarctic Peninsula (Christ et al., 2015; Domack et al., 2001; Reilly et al., 2016; Shevenell et al., 1996), which is generally interpreted as an equatorial shift in the westerlies (negative phase of SAM). Across the Pacific Ocean in Patagonia,
525 Moy et al., (2008) present a high resolution record that spans the LIA, and identifies the period from 400-150 yr BP as an intensification of wind at 51° S, and although our record does not cover this interval, this comparison to Fiordland suggests a breakdown in zonal symmetry across the Pacific during the LIA.

Overall, SHWW behaviour during the LIA appears to be generally characterised by a northward shift, associated with a negative phase of the SAM. The regional response of climate in southern New Zealand to variations in both the SAM and
530 ENSO may be contributing to local differences. In addition, comparison of SHWW reconstructions from New Zealand to those in southern South America and the western Antarctic Peninsula suggest that zonal symmetry in the winds across the Pacific breaks down during the LIA, although further high resolution records of wind strength with robust chronologies are required to fully assess this. Zonal symmetry of the winds during the Holocene is important to understand because we know that the position of the winds on longer timescales can affect global carbon cycling, where a northward (southward) position
535 of the SHWW is generally associated with decreased (increased) atmospheric CO_2 (Anderson et al., 2009; Sigman et al., 2010; Skinner et al., 2010; Toggweiler et al., 2006).

6 Conclusions

We reconstructed past changes in the strength of the SHWW using a sediment core recovered from a silled inlet at the Auckland Islands, located in the SAZ south of New Zealand, within the core of the modern SHWW. Modern process studies
540 reveal that increased summer precipitation and wind strength induces rapid and complete vertical mixing of fjord waters, reduced fjord salinity, and triggers return flow of saline shelf water rich in OM_{mar} at depth.



Downcore changes in magnetic susceptibility, oxygen and carbon stable isotopes of benthic foraminifera, and bulk organic carbon isotopes and atomic C/N provide evidence for the Holocene paleoenvironmental evolution of Hanfield Inlet. Seismic data and a transition from lacustrine to marine sediments reveals the post-glacial evolution of Hanfield Inlet, where marine incursion into a paleolake occurred around 10,000- 9,000- yr BP, based on local sea level reconstructions (Clement et al., 2016; Dlabola et al., 2015). Magnetic susceptibility, bulk organic $\delta^{13}\text{C}$ and atomic C/N indicate increased SHWW influence from 1,600-900 yr BP, consistent with previous palynological reconstructions of precipitation wind strength at the Auckland Islands (McGlone et al., 2000; Turney et al., 2016). Bulk organic $\delta^{13}\text{C}$, and wt% TN and TOC indicate increased productivity from 900-500 yr BP, associated with increased fjord stratification due to decreased influence of SHWW. Comparison of the Auckland Islands record of SHWW with another from Fiordland, New Zealand (Knudson et al., 2011) indicate that the SHWW field shifted southward from ~1,400-1,000 yr BP and northward towards southern New Zealand at ~900 yr BP. From ~900-750 yr BP, roughly coincident with the beginning of the LIA, the winds shifted further northward and this is likely associated with dominance of the negative phase of the SAM during this time (Abram et al., 2014; Villalba et al., 1997, 2012). Comparison with records from similar latitudes in southern South America (Aracena et al., 2015; Moy et al., 2008) and the WAP (Shevenell et al., 2011) indicate a late Holocene intensification of the SHWW across the Southern Ocean, indicating that the winds may have been zonally symmetric across the Pacific Ocean from at least 1,600-900 yr BP, and asymmetric after this.

Sub-millennial scale variations in the stable oxygen and carbon isotopes of benthic foraminifera from Hanfield Inlet are controlled indirectly through the influence of SHWW on shelf and fjord hydrography. The strength, symmetry and latitudinal position of the SHWW (modulated by both the SAM and ENSO) exerts a dominant control on upwelling of nutrient- and carbon- rich water masses along fronts of the ACC, which are exported northwards to the New Zealand continental shelf. Depleted foraminifer $\delta^{13}\text{C}$ and $\delta^{18}\text{O}$ is related to increased wind-derived fjord precipitation (decreased salinity and decreased $\delta^{13}\text{C}_{\text{DIC}}$ due to increased respiration of OM_{terr}), and input of warm shelf waters with depleted $\delta^{13}\text{C}_{\text{DIC}}$ as a result of enhanced wind-driven upwelling and northward export of SAMW south of New Zealand. Intensified SHWW during the late Holocene coincides with increased teleconnections between the Tropical Pacific and high latitudes, and this study provides the first evidence for such teleconnections being present in the southwest Pacific Ocean.

7 Author Contribution

I. Browne, C. Moy, L. Curtin, and A. Gorman carried out field work. I. Browne and L. Curtin carried out stable isotope analysis of water, particulates, and sediment. I. Browne and H. Neil carried out foraminifer stable isotope analysis. I. Browne prepared the manuscript with contributions from all co-authors.



8 Competing Interests

The authors declare that they have no conflict of interest.

9 Acknowledgements

The authors gratefully acknowledge support from a Royal Society of New Zealand Marsden Fast Start and New Zealand
575 Antarctic Research Institute (NZARI) funding to C. Moy. Radiocarbon analyses were performed at the Lawrence Livermore
Laboratory. Seismic data were processed using an academic licence for GLOBE Claritas by B. Ross. NCEP Reanalysis data
provided by the NOAA/OAR/ESRL PSD, Boulder, Colorado, USA, from their Web site at <http://www.esrl.noaa.gov/psd/>.
We would like to thank B. Hayward for help with identification of benthic foraminifera, T. Max at NIWA for analysing
foraminifer stable isotopes, and R. Van Hale, K. Currie and C. Aebig at the University of Otago for analysing the isotopic
580 composition of water, particulates and sediment. Special thanks to the crew and scientific party on Auckland Islands cruises
14PL001 and 15PL001.

10 References

- Abram, N. J., Mulvaney, R., Vimeux, F., Phipps, S. J., Turner, J. and England, M. H.: Evolution of the Southern Annular
Mode during the past millennium, *Nat. Clim. Chang.*, 4(7), 564–569, doi:10.1038/nclimate2235, 2014.
- 585 Adams, C. J.: Age of the volcanoes and granite basement of the Auckland Islands, Southwest Pacific, *New Zeal. J. Geol.*
Geophys., 26(3), 227–237, doi:10.1080/00288306.1983.10422237, 1983.
- Altabet, M. A. and Francois, F.: Sedimentary nitrogen isotopic ratio as a recorder for surface ocean nitrate utilization.,
Biogeochem. Cycles., 8(1), 103–116, doi:10.1029/93GB03396, 1994.
- Anderson, B. E., Ali, S., Bradtmiller, L. I., Neilsen, S. H. H., Fleisher, M. Q., Anderson, B. E. and Burckle, L. H.: Wind-
590 Driven upwelling in the Southern Ocean and the Deglacial rise in Atmospheric CO₂, *Science* (80-.), 323(March), 1443–
1448, doi:10.1126/science.1167441, 2009.
- Aracena, C., Kilian, R., Lange, C. B., Bertrand, S., Lamy, F., Arz, H. W., De Pol-Holz, R., Baeza, O., Pantoja, S. and Kissel,
C.: Holocene variations in productivity associated with changes in glacier activity and freshwater flux in the central basin of
the Strait of Magellan, *Palaeogeogr. Palaeoclimatol. Palaeoecol.*, 436, 112–122, doi:10.1016/j.palaeo.2015.06.023, 2015.
- 595 Archer, C. L. and Caldeira, K.: Historical trends in the jet streams, *Geophys. Res. Lett.*, 35(8), L08803,
doi:10.1029/2008GL033614, 2008.
- Ariztegui, D., Gilli, A., Anselmetti, F. S., Goni, R. A., Belardi, J. B. and Espinosa, S.: Lake-level changes in central
Patagonia (Argentina): crossing environmental thresholds for Lateglacial and Holocene human occupation, *J. Quat. Sci.*,
25(7), 1092–1099, doi:10.1002/jqs, 2010.
- 600 Bertler, N. A. N., Mayewski, P. A. and Carter, L.: Cold conditions in Antarctica during the Little Ice Age - Implications for



- abrupt climate change mechanisms, *Earth Planet. Sci. Lett.*, 308(1–2), 41–51, doi:10.1016/j.epsl.2011.05.021, 2011.
- Blaauw, M. and Christen, J. A.: Flexible paleoclimate age-depth models using an autoregressive gamma process, *Bayesian Anal.*, 6(3), 457–474, doi:10.1214/11-BA618, 2011.
- Bostock, H. C., Hayward, B. W., Neil, H. L., Sabaa, A. T. and Scott, G. H.: Changes in the position of the Subtropical Front south of New Zealand since the last glacial period, *Paleoceanography*, 30, 824–844, doi:10.1002/2014PA002652. Received, 2015.
- Boyer, T. P., Antonov, J. I., Baranova, O. K., Coleman, C., Garcia, H. E., Grodsky, A., Johnson, D. R., Locarnini, R. A., Mishonov, A. V., O'Brien, T. D., Paver, C. R., Reagan, J. R., Seidov, D., Smolyar, I. V. and Zweng, M. M.: *World Ocean Database 2013, NOAA Atlas NESDIS 72*, edited by S. Levitus and A. V. Mishonov, NOAA, Silver Spring, MD., 2013.
- 610 Carter, L., McCave, I. N. and Williams, M. J. M.: Circulation and Water Masses of the Southern Ocean: A Review, in *Developments in Earth and Environmental Sciences*, vol. 8, edited by F. Florindo and M. Sigert, pp. 85–114, Elsevier., 2009.
- Chiang, J. C. H., Lee, S. Y., Putnam, A. E. and Wang, X.: South Pacific Split Jet, ITCZ shifts, and atmospheric North-South linkages during abrupt climate changes of the last glacial period, *Earth Planet. Sci. Lett.*, 406, 233–246, doi:10.1016/j.epsl.2014.09.012, 2014.
- 615 Christ, A. J., Talaia-Murray, M., Elking, N., Domack, E. W., Leventer, A., Lavoie, C., Brachfeld, S., Yoo, K. C., Gilbert, R., Jeong, S. M., Petrushak, S., Wellner, J., Balco, G., Brachfeld, S., de Batist, M., Domack, E., Gordon, A., Haran, A., Henriot, J. P., Huber, B., Ishman, S., Jeong, S., King, M., Lavoie, C., Leventer, A., McCormick, M., Mosley-Thompson, E., Pettit, E., Scambos, T., Smith, C., Thompson, L., Truffer, M., van Dover, C., Vernet, M., Wellner, J., Yu, K. and Zagorodnov, V.: Late Holocene glacial advance and ice shelf growth in Barilari Bay, Graham Land, West Antarctic Peninsula, *Bull. Geol. Soc. Am.*, 127(1–2), 297–315, doi:10.1130/B31035.1, 2015.
- 620 Clement, A. J. H., Whitehouse, P. L. and Sloss, C. R.: An examination of spatial variability in the timing and magnitude of Holocene relative sea-level changes in the New Zealand archipelago, *Quat. Sci. Rev.*, 131, 73–101, doi:10.1016/j.quascirev.2015.09.025, 2016.
- Cook, A. J., Holland, P. R., Meredith, M. P., Murray, T., Luckman, A. and Vaughan, D. G.: Ocean forcing of glacier retreat in the western Antarctic Peninsula, *Science* (80-.), 353(6296), 283–286, 2016.
- 625 Cook, E. R., Palmer, J. G. and Arrigo, R. D. D.: Evidence for a “ Medieval Warm Period ” in a 1 , 100 year tree-ring reconstruction of past austral summer temperatures in New Zealand, *Geophys. Res. Lett.*, 29(14), 14–17, doi:10.1029/2001GL014580, 2002.
- Dinniman, M. S., Klinck, J. M. and Hofmann, E. E.: Sensitivity of circumpolar deep water transport and ice shelf basal melt along the west Antarctic Peninsula to changes in the winds, *J. Clim.*, 25(14), 4799–4816, doi:10.1175/JCLI-D-11-00307.1, 2012.
- 630 Dlabola, E. K., Wilson, G. S., Gorman, A. R., Riesselman, C. R. and Moy, C. M.: A post-glacial relative sea-level curve from Fiordland, New Zealand, *Glob. Planet. Change*, 131, 104–114, doi:10.1016/j.gloplacha.2015.05.010, 2015.
- Domack, E., Leventer, A., Dunbar, R., Taylor, F., Brachfeld, S., Sjunneskog, C. and Party, O. L. 178 S.: Chronology of the



- 635 Palmer Deep site , Antarctic Peninsula : a Holocene palaeoenvironmental reference for the circum-Antarctic, *The Holocene*, 1, 1–9, 2001.
- Fleming, C. A., Mildenhall, D. C. and Moar, N. T.: Quaternary sediments and plant microfossils from Enderby Island, Auckland Islands, *J. R. Soc. New Zeal.*, 6(4), 433–458, doi:10.1080/03036758.1976.10421484, 1976.
- Fletcher, M.-S. and Moreno, P. I.: Have the Southern Westerlies changed in a zonally symmetric manner over the last 14,000 years? A hemisphere-wide take on a controversial problem, *Quat. Int.*, 253, 32–46, doi:10.1016/j.quaint.2011.04.042, 2012.
- 640 Garreaud, R.: Precipitation and Circulation Covariability in the Extratropics, *J. Clim.*, 20(18), 4789–4797, doi:10.1175/JCLI4257.1, 2007.
- Garreaud, R., Lopez, P., Minvielle, M. and Rojas, M.: Large-scale control on the Patagonian climate, *J. Clim.*, 26(1), 215–230, doi:10.1175/JCLI-D-12-00001.1, 2013.
- 645 Gellatly, A. F., Chinn, T. J. H. and Rothlisberger, F.: Holocene glacier variations in New Zealand: A review, *Quat. Sci. Rev.*, 7(2), 227–242, doi:10.1016/0277-3791(88)90008-X, 1988.
- Gibbs, M. T., Bowman, M. J. and Dietrich, D. E.: Maintenance of Near-Surface Stratification in Doubtful Sound, a New Zealand Fjord, *Estuar. Coast. Shelf Sci.*, 51(6), 683–704, doi:10.1006/ecss.2000.0716, 2000.
- Graham, D. W., Corliss, B. H., Bender, M. L. and Keigwin, L. D.: Carbon and oxygen isotopic disequilibria of recent deep-sea benthic foraminifera*, *Mar. Micropaleontol.*, 6, 483–497, 1981.
- 650 Grossman, E. L.: Stable isotope fractionation in live benthic foraminifera from the southern California Borderland, *Palaeogeogr. Palaeoclimatol. Palaeoecol.*, 47(3–4), 301–327, doi:10.1016/0031-0182(84)90100-7, 1984.
- Sen Gupta, A. and England, M. H.: Coupled ocean-atmosphere-ice response to variations in the southern annular mode, *J. Clim.*, 19(18), 4457–4486, doi:10.1175/JCLI3843.1, 2006.
- 655 Hald, M. and Vorren, T. O.: Foraminiferal stratigraphy and environment of Late Weichselian deposits on the continental shelf off Troms, northern Norway, *Mar. Micropaleontol.*, 12, 129–160, doi:10.1016/0377-8398(87)90018-1, 1987.
- Hall, A. and Visbeck, M.: Synchronous variability in the Southern Hemisphere atmosphere, sea ice, and ocean resulting from the annular mode, *J. Clim.*, 15(21), 3043–3057, 2002.
- Haug, G. H., Hughen, K. A., Sigman, D. M., Peterson, L. C. and Röhl, U.: Southward migration of the intertropical convergence zone through the Holocene., *Science*, 293(5533), 1304–8, doi:10.1126/science.1059725, 2001.
- 660 Hinojosa, J. L., Moy, C. M., Stirling, Claudine, H., Wilson, G. S. and Eglinton, Timothy, I.: Carbon cycling and burial in New Zealand’ s fjords, *Geochemistry Geophys. Geosystems*, 15, 4047–4063, doi:10.1002/2014GC005433, 2014.
- Hogg, A. G., Hua, Q., Blackwell, P. G., Niu, M., Buck, C. E., Guilderson, T. P., Heaton, T. J., Palmer, J. G., Reimer, P. J., Reimer, R. W., Turney, C. S. M. and Zimmerman, S. R. H.: SHCAL13 Southern Hemisphere calibration, 0–50,000 years
- 665 CAL BP, *Radiocarbon*, 55(4), 1889–1903, 2013.
- Hut, G.: Consultant’s group meeting on stable isotope reference samples for geochemical and hydrological investigations., 1987.
- Kalnay, E., Kanamitsu, M., Kistler, R., Collins, W., Deaven, D., Gandin, L., Iredell, M., Saha, S., White, G., Woollen, J.,



- Zhu, Y., Leetmaa, A., Reynolds, R., Chelliah, M., Ebisuzaki, W., Higgins, W., Janowiak, J., Mo, K. C., Ropelewski, C.,
670 Wang, J., Jenne, R., Joseph, D.: The NCEP/NCAR 40-year reanalysis project, *Bull. Amer. Meteor. Soc.*, 77, 437–470, 1996.
- Kilian, R. and Lamy, F.: A review of Glacial and Holocene paleoclimate records from southernmost Patagonia (49–55°S),
Quat. Sci. Rev., 53, 1–23, doi:10.1016/j.quascirev.2012.07.017, 2012.
- Kim, S.-T. and O’Neil, J. R.: Equilibrium and nonequilibrium oxygen isotope effects in synthetic carbonates, *Geochim.
Cosmochim. Acta*, 61(16), 3461–3475, 1997.
- 675 Knudson, K. P., Hendy, I. L. and Neil, H. L.: Re-examining Southern Hemisphere westerly wind behavior: insights from a
late Holocene precipitation reconstruction using New Zealand fjord sediments, *Quat. Sci. Rev.*, 30(21–22), 3124–3138,
doi:10.1016/j.quascirev.2011.07.017, 2011.
- Lamy, F., Kilian, R., Arz, H. W., Francois, J.-P., Kaiser, J., Prange, M. and Steinke, T.: Holocene changes in the position and
intensity of the southern westerly wind belt, *Nat. Geosci.*, 3(10), 695–699, doi:10.1038/ngeo959, 2010.
- 680 Landschützer, P., Gruber, N., Haumann, F. A., Rödenbeck, C., Bakker, D. C. E., Heuven, S. Van, Hoppema, M., Metzl, N.,
Sweeney, C. and Takahashi, T.: The reinvigoration of the Southern Ocean carbon sink, *Science* (80-.), 349(6253), 1221–
1224, doi:10.1126/science.aab2620, 2015.
- Lenton, A., Tilbrook, B., Law, R. M., Bakker, D., Doney, S. C., Gruber, N., Ishii, M., Hoppema, M., Lovenduski, N. S.,
Matear, R. J., McNeil, B. I., Metzl, N., Fletcher, S. E. M., Monteiro, P. M. S., Rodenbeck, C., Sweeney, C. and Takahashi,
685 T.: Sea-air CO₂ fluxes in the Southern Ocean for the period 1990–2009, *Biogeosciences*, 10(6), 4037–4054, doi:10.5194/bg-
10-4037-2013, 2013.
- Lorrey, A., Williams, P., Salinger, J., Martin, T., Palmer, J., Fowler, A., Zhao, J. and Neil, H.: Speleothem stable isotope
records interpreted within a multi-proxy framework and implications for New Zealand palaeoclimate reconstruction, , 187,
52–75, doi:10.1016/j.quaint.2007.09.039, 2008.
- 690 Lorrey, A., Fauchereau, N., Stanton, C., Chappell, P., Phipps, S., Mackintosh, A., Renwick, J., Goodwin, I. and Fowler, A.:
The Little Ice Age climate of New Zealand reconstructed from Southern Alps cirque glaciers: A synoptic type approach,
Clim. Dyn., 42(11–12), 3039–3060, doi:10.1007/s00382-013-1876-8, 2014.
- Lovenduski, N., Gruber, N. and Doney, S. .: Toward a mechanistic understanding of the decadal trends in the Southern
Ocean carbon sink, *Global Biogeochem. Cycles*, 22, 1–9, doi:10.1029/2007GB003139, 2008.
- 695 Lovenduski, N. S. and Gruber, N.: Impact of the Southern Annular Mode on Southern Ocean circulation and biology,
Geophys. Res. Lett., 32(11), 1–4, doi:10.1029/2005GL022727, 2005.
- Lynch-Stieglitz, J., Curry, W. B. and Slowey, N.: A geostrophic transport estimate for the Florida Current from the oxygen
isotope composition of benthic foraminifera, , 14(3), 360–373, 1999.
- Mackensen, A., Grobe, H., Kuhn, G. and Fiitterer, D. K.: Benthic foraminiferal assemblages from the eastern Weddell Sea
700 between 68 and 73° S: Distribution, ecology and fossilization potential, *Mar. Micropaleontol.*, 16, 241–283,
doi:10.1016/0377-8398(90)90006-8, 1990.
- Mackensen, A., Schumacher, S., Radke, J. and Schmidt, D. N.: Microhabitat preferences and stable carbon isotopes of



- endobenthic foraminifera : clue to quantitative reconstruction of oceanic new production ?, *Mar. Micropaleontol.*, 40, 233–258, 2000.
- 705 Marchitto, T. M., Curry, W. B., Lynch-Stieglitz, J., Bryan, S. P., Cobb, K. M. and Lund, D. C.: Improved oxygen isotope temperature calibrations for cosmopolitan benthic foraminifera, *Geochim. Cosmochim. Acta*, 130, 1–11, doi:10.1016/j.gca.2013.12.034, 2014.
- Marshall, G. J.: Trends in the Southern Annular Mode from observations and reanalyses, *J. Clim.*, 16(24), 4134–4143, doi:1, 2003.
- 710 Martinson, D. G., Stammerjohn, S. E., Iannuzzi, R.A., Smith, R. C. and Vernet, M.: Western Antarctic Peninsula physical oceanography and spatio-temporal variability, *Deep Sea Res. Part II Top. Stud. Oceanogr.*, 55(18–19), 1964–1987, doi:10.1016/j.dsr2.2008.04.038, 2008.
- Mayewski, P. A., Rohling, E. E., Curt Stager, J., Karlén, W., Maasch, K. a., David Meeker, L., Meyerson, E. a., Gasse, F., van Kreveld, S., Holmgren, K., Lee-Thorp, J., Rosqvist, G., Rack, F., Staubwasser, M., Schneider, R. R. and Steig, E. J.:
- 715 Holocene climate variability, *Quat. Res.*, 62(3), 243–255, doi:10.1016/j.yqres.2004.07.001, 2004.
- McCorkle, D., Keigwin, L., Corliss, B. and Emerson, S.: The influence of microhabitats on the carbon isotopic composition of deep-sea benthic foraminifera, *Paleoceanography*, 5(2), 161–185 [online] Available from: <http://onlinelibrary.wiley.com/doi/10.1029/PA005i002p00161/full>, 1990.
- McCorkle, D. C., Corliss, B. H. and Farnham, C. A.: Vertical distributions and stable isotopic compositions of live (stained)
- 720 benthic foraminifera from the North Carolina and California continental margins, *Deep. Res. Part I Oceanogr. Res. Pap.*, 44(6), 983–1024, doi:10.1016/S0967-0637(97)00004-6, 1997.
- McFadgen, B. G. and Yaldwyn, J. C.: Holocene sand dunes on Enderby Island, Auckland Islands, New Zeal. *J. Geol. Geophys.*, 27(1), 27–33, doi:10.1080/00288306.1984.10422289, 1984.
- McGlone, M. S.: The Late Quaternary peat, vegetation and climate history of the Southern Oceanic Islands of New Zealand,
- 725 *Quat. Sci. Rev.*, 21(4–6), 683–707, doi:10.1016/S0277-3791(01)00044-0, 2002.
- McGlone, M. S. and Moar, N. T.: Pollen vegetation relationships on the subantarctic Auckland Islands, New Zealand, *Rev. Palaeobot. Palynol.*, 96(3–4), 317–338, doi:10.1016/S0034-6667(96)00058-9, 1997.
- McGlone, M. S., Wilmshurst, J. M. and Wiser, S. K.: Lateglacial and Holocene vegetation and climatic change on Auckland Island, Subantarctic New Zealand, *The Holocene*, 10(6), 719–728, doi:10.1191/09596830094962, 2000.
- 730 McGlone, M. S., Turney, C. S. M., Wilmshurst, J. M., Renwick, J. and Pahnke, K.: Divergent trends in land and ocean temperature in the Southern Ocean over the past 18,000 years, *Nat. Geosci.*, 3(9), 622–626, doi:10.1038/ngeo931, 2010.
- McNeil, B. I., Metzl, N., Key, R. M., Matear, R. J. and Corbiere, A.: An empirical estimate of the Southern Ocean air-sea CO₂ flux, *Global Biogeochem. Cycles*, 21(3), 1–16, doi:10.1029/2007GB002991, 2007.
- Menviel, L., Timmermann, A., Mouchet, A. and Timm, O.: Climate and marine carbon cycle response to changes in the
- 735 strength of the Southern Hemispheric westerlies, *Paleoceanography*, 23(4), 1–10, doi:10.1029/2008PA001604, 2008.
- Metzl, N.: Decadal increase of oceanic carbon dioxide in Southern Indian Ocean surface waters (1991–2007), *Deep. Res.*



- Part II Top. Stud. Oceanogr., 56(8–10), 607–619, doi:10.1016/j.dsr2.2008.12.007, 2009.
- Metzl, N., Tilbrook, B. and Poisson, A.: The annual fCO₂ cycle and the air-sea CO₂ flux in the sub-Antarctic Ocean, *Tellus, Ser. B Chem. Phys. Meteorol.*, 51(4), 849–861, doi:10.1034/j.1600-0889.1999.t01-3-00008.x, 1999.
- 740 Metzl, N., Brunet, C., Jabaud-Jan, A., Poisson, A. and Schauer, B.: Summer and winter air-sea CO₂ fluxes in the Southern Ocean, *Deep. Res. Part I Oceanogr. Res. Pap.*, 53(9), 1548–1563, doi:10.1016/j.dsr.2006.07.006, 2006.
- Meyers, P. A. and Teranes, J. L.: Sediment Organic Matter, in *Tracking Environmental Change Using Lake Sediments*, vol. 2, edited by W. M. Last and J. P. Smol, pp. 239–269, Kluwer Academic Publishers., 2001.
- Moreno, P. I., Francois, J. P., Villa-Martinez, R. P. and Moy, C. M.: Millennial-scale variability in Southern Hemisphere
745 westerly wind activity over the last 5000 years in SW Patagonia, *Quat. Sci. Rev.*, 28, 25–38, doi:10.1016/j.quascirev.2008.10.009, 2009.
- Mosley-Thompson, E., Thompson, L. G., Grootes, P. M. and Gundestrup, N.: Little Ice Age (Neoglacial) paleoenvironmental conditions at Siple Station, Antarctica, *Ann. Glaciol.*, 14, 199–204, 1990.
- Moy, C. M., Dunbar, R. B., Moreno, P. I., Francois, J.-P., Villa-Martínez, R., Mucciarone, D. M., Guilderson, T. P. and
750 Garreaud, R. D.: Isotopic evidence for hydrologic change related to the westerlies in SW Patagonia, Chile, during the last millennium, *Quat. Sci. Rev.*, 27(13–14), 1335–1349, doi:10.1016/j.quascirev.2008.03.006, 2008.
- O’Neil, J. R., Clayton, R. N. and Mayeda, T. K.: Oxygen Isotope Fractionation in Divalent Metal Carbonates, *J. Chem. Phys.*, 51(12), 5547–5558, doi:10.1063/1.1671982, 1969.
- Palter, J. B., Sarmiento, J. L., Gnanadesikan, A., Simeon, J. and Slater, R. D.: Fueling export production: Nutrient return
755 pathways from the deep ocean and their dependence on the Meridional Overturning Circulation, *Biogeosciences*, 7(11), 3549–3568, doi:10.5194/bg-7-3549-2010, 2010.
- Pickrill, R. : Circulation and sedimentation of suspended particulate matter in New Zealand fjords, *Mar. Geol.*, 74(1–2), 21–39, doi:10.1016/0025-3227(87)90003-X, 1987.
- Putnam, A. E., Schaefer, J. M., Barrell, D. J. A., Vandergoes, M., Denton, G. H., Kaplan, M. R., Finkel, R. C., Schwartz, R.,
760 Goehring, B. M. and Kelley, S. E.: Quaternary Geochronology In situ cosmogenic New Zealand Be production-rate calibration from the Southern Alps , *Quat. Geochronol.*, 5(4), 392–409, doi:10.1016/j.quageo.2009.12.001, 2010.
- Le Quéré, C., Rödenbeck, C., Buitenhuis, E. T., Conway, T. J., Langenfelds, R., Gomez, A., Labuschagne, C., Ramonet, M., Nakazawa, T., Metzl, N., Gillett, N. and Heimann, M.: Saturation of the southern ocean CO₂ sink due to recent climate change., *Science*, 316(5832), 1735–8, doi:10.1126/science.1136188, 2007.
- 765 Ravelo, A. C. and Hillaire-Marcel, C.: The Use of Oxygen and Carbon Isotopes of Foraminifera in Paleooceanography, in *Developments in Marine Geology*, vol. 1, pp. 735–764, Elsevier B.V., 2007.
- Reilly, B. T., Natter, C. J. and Brachfeld, S. A.: Holocene glacial activity in Barilari Bay, west Antarctic Peninsula, tracked by magnetic mineral assemblages: Linking ice, ocean, and atmosphere, *Geochemistry Geophys. Geosystems*, 17, 2825–2834, doi:10.1002/2016GC006406, 2016.
- 770 Rhodes, R. H., Bertler, N. A. N., Baker, J. A., Steen-Larsen, H. C., Sneed, S. B., Morgenstern, U. and Johnsen, S. J.: Little



- Ice Age climate and oceanic conditions of the Ross Sea, Antarctica from a coastal ice core record, *Clim. Past*, 8(4), 1223–1238, doi:10.5194/cp-8-1223-2012, 2012.
- Sarmiento, J. L., Gruber, N., Brzezinski, M. A. and Dunne, J. P.: High-latitude controls of thermocline nutrients and low latitude biological productivity., *Nature*, 427(6969), 56–60, doi:10.1038/nature10605, 2004.
- 775 Saunders, K. M., Kamenik, C., Hodgson, D. A., Hunziker, S., Siffert, L., Fischer, D., Fujak, M., Gibson, J. A. E. and Grosjean, M.: Late Holocene changes in precipitation in northwest Tasmania and their potential links to shifts in the Southern Hemisphere westerly winds, *Glob. Planet. Change*, 92–93, 82–91, doi:10.1016/j.gloplacha.2012.04.005, 2012.
- Scott, D. B., Medioli, F. S. and Schafer, C. T.: *Monitoring in Coastal Environments Using Foraminifera and Thecamoebian Indicators*, Cambridge University Press, New York., 2001.
- 780 Shackleton, N. J.: Attainment of isotopic equilibrium between ocean water and the benthonic foraminifera genus *Uvigerina*: isotopic changes in the ocean during the last glacial, *Colloq. Int. du C. N. R. S*, 219, 203–209, 1974.
- Shevenell, A., Domack, E. W. and Kernan, G.: Record of Holocene paleoclimate change along the Antarctic Peninsula: evidence from glacial marine sediments, Lallenmand Fjord, *Pap. Proc. R. Soc. Tasmania*, 130(2), 55–64, 1996.
- Shevenell, A. E., Ingalls, A. E., Domack, E. W. and Kelly, C.: Holocene Southern Ocean surface temperature variability west of the Antarctic Peninsula., *Nature*, 470, 250–4, doi:10.1038/nature09751, 2011.
- 785 Shindell, D. T. and Schmidt, G. A.: Southern Hemisphere climate response to ozone changes and greenhouse gas increases, *Geophys. Res. Lett.*, 31(18), doi:10.1029/2004GL020724, 2004.
- Sigman, D. M., Hain, M. P. and Haug, G. H.: The polar ocean and glacial cycles in atmospheric CO₂ concentration, *Nature*, 466(7302), 47–55, doi:10.1038/nature09149, 2010.
- 790 Skinner, L. C., Fallon, S., Waelbroeck, C., Michel, E. and Barker, S.: Ventilation of the Deep Southern Ocean and Deglacial CO₂ Rise, *Science* (80-.), 328(5982), 1147–1151, doi:10.1126/science.1183627, 2010.
- Smith, R. O., Vennell, R., Bostock, H. C. and Williams, M. J. M.: Interaction of the subtropical front with topography around southern New Zealand, *Deep. Res. Part I Oceanogr. Res. Pap.*, 76, 13–26, doi:10.1016/j.dsr.2013.02.007, 2013.
- Stanton, B. R.: Some Oceanographic New Zealand Fjords Observations in the, Estaurine, Coast. Shelf Sci., 19, 89–104, 795 1984.
- Stuiver, M. and Reimer, P. J.: Extended 14C data base and revised CALIB 3.0 14C age calibration program, *Radiocarbon*, 35(1), 215–230, 1993.
- Takahashi, T., Sutherland, S. ., Sweeney, C., Poisson, A., Metzl, N., Tilbrook, B., Bates, N., Wanninkhof, R., Feely, R. A., Sabine, C., Olafsson, J. and Nojiri, Y.: Global sea – air CO₂ flux based on climatological surface ocean pCO₂ , and seasonal 800 biological and temperature effects, *Deep. Rearch II*, 49, 1601–1622, 2002.
- Takahashi, T., Sutherland, S. C., Wanninkhof, R., Sweeney, C., Feely, R. A., Chipman, D. W., Hales, B., Friederich, G., Chavez, F., Sabine, C., Watson, A., Bakker, D. C. E., Schuster, U., Metzl, N., Yoshikawa-Inoue, H., Ishii, M., Midorikawa, T., Nojiri, Y., Kortzinger, A., Steinhoff, T., Hoppema, M., Olafsson, J., Arnarson, T. S., Tilbrook, B., Johannessen, T., Olsen, A., Bellerby, R., Wong, C. S., Delille, B., Bates, N. R. and de Baar, H. J. W.: Climatological mean and decadal



- 805 change in surface ocean pCO₂, and net sea-air CO₂ flux over the global oceans, *Deep. Res. Part II Top. Stud. Oceanogr.*,
56(8–10), 554–577, doi:10.1016/j.dsr2.2008.12.009, 2009.
- Takahashi, T. C., Sweeney, C., Hales, B., Chipman, D. W., Newberger, T., Goddard, J. G., Iannuzzi, R. A. and Sutherland,
S. C.: The changing carbon cycle in the Southern Ocean, *Oceanography*, 25(3), 26–37, 2012.
- Thompson, D. W. J. and Solomon, S.: Interpretation of Recent Southern Hemisphere Climate Change, *Science* (80-.),
810 296(2002), 895–899, doi:10.1126/science.1069270, 2002.
- Toggweiler, J. R., Russell, J. L. and Carson, S. R.: Midlatitude westerlies, atmospheric CO₂, and climate change during the
ice ages, *Paleoceanography*, 21(2), PA2005, doi:10.1029/2005PA001154, 2006.
- Trenberth, K. E.: Storm tracks in the Southern Hemisphere, *J. Atmos. Sci.*, 48(19), 2159–2178, doi:10.1002/2014JC009990,
1991.
- 815 Turney, C., Jones, R., Fogwill, C., Hatton, J., Williams, A. N., Hogg, A., Thomas, Z., Palmer, J. and Mooney, S.: A 250 year
periodicity in Southern Hemisphere westerly winds over the last 2600 years, *Clim. Past Discuss.*, 11(3), 2159–2180,
doi:10.5194/cpd-11-2159-2015, 2015.
- Turney, C. S. M., McGlone, M., Palmer, J., Fogwill, C., Hogg, A., Thomas, Z. O. E. A., Lipson, M., Wilmshurst, J. M.,
Fenwick, P., Jones, R. T., Hines, B. E. N. and Clark, G. F.: Intensification of Southern Hemisphere westerly winds 2000 –
820 1000 years ago : evidence from the subantarctic Campbell and Auckland Islands (52 – 50 ° S), *J. Quat. Sci.*, 31(1), 12–19,
doi:10.1002/jqs.2828, 2016.
- Turney, C. S. M., Wilmshurst, J. M., Jones, R. T., Wood, J. R., Palmer, J. G., Hogg, A. G., Fenwick, P., Crowley, S. F.,
Privat, K. and Thomas, Z.: Reconstructing atmospheric circulation over southern New Zealand : Establishment of modern
westerly air flow 5500 years ago and implications for Southern Hemisphere Holocene climate change, *Quat. Sci. Rev.*, 159,
825 77–87, doi:10.1016/j.quascirev.2016.12.017, 2017.
- Ummenhofer, C. C. and England, M. H.: Interannual Extremes in New Zealand Precipitation Linked to Modes of Southern,
J. Clim., 20, 5418–5440, doi:10.1175/2007JCLI1430.1, 2007.
- Ummenhofer, C. C., Sen Gupta, A. and England, M. H.: Causes of late twentieth-century trends in New Zealand
precipitation, *J. Clim.*, 22(1), 3–19, doi:10.1175/2008JCLI2323.1, 2009.
- 830 Villalba, R., Cook, E. R., D’Arrigo, R. D., Jacoby, G. C., Jones, P. D., Salinger, M. J. and Palmer, J.: Sea-level pressure
variability around Antarctica since A.D. 1750 inferred from subantarctic tree-ring records, *Clim. Dyn.*, 13(6), 375–390,
doi:10.1007/s003820050172, 1997.
- Villalba, R., Lara, A., Masiokas, M. H., Urrutia, R., Luckman, B. H., Marshall, G. J., Mundo, I. A., Christie, D. A., Cook, E.
R., Neukom, R., Allen, K., Fenwick, P., Boninsegna, J. A., Srur, A. M., Morales, M. S., Araneo, D., Palmer, J. G., Cuq, E.,
835 Aravena, J. C., Holz, A. and LeQuesne, C.: Unusual Southern Hemisphere tree growth patterns induced by changes in the
Southern Annular Mode, *Nat. Geosci.*, 5(11), 793–798, doi:10.1038/ngeo1613, 2012.
- Waldmann, N., Ariztegui, D., Anselmetti, F. S., Austin, J. A. J., Moy, C. M., Stern, C., Recasens, C. and Dunbar, R. B.:
Holocene climatic fluctuations and positioning of Southern Hemisphere westerlies in Tierra del Fuego (54S), Patagonia, J.



Quat. Sci., 25(7), 1063–1075, doi:10.1002/jqs, 2010.

840 Walinsky, S. E., Prah, F. G., Mix, A. C., Finney, B. P., Jaeger, J. M. and Rosen, G. P.: Distribution and composition of organic matter in surface sediments of coastal Southeast Alaska, Cont. Shelf Res., 29(13), 1565–1579, doi:10.1016/j.csr.2009.04.006, 2009.

Wetzel, P., Winguth, A. and Maier-Reimer, E.: Sea-to-air CO₂ flux from 1948 to 2003: A model study, Global Biogeochem. Cycles, 19(2), 1–19, doi:10.1029/2004GB002339, 2005.

845



850

Table 1. All samples used in the current study. G= grab sample; CTD= Conductivity, Temperature, Depth sample; B= box-core sample; P= piston-core sample. Number indicates the order of sampling at that site. C/N= bulk carbon and nitrogen analysis; FI= benthic foraminiferal stable carbon and oxygen isotope geochemistry; WI= stable carbon and oxygen isotope geochemistry of water; PP= physical properties. All samples were collected from R/V *Polaris II* on expeditions 14PL001 and 15PL001.

| Cruise | Latitude | Longitude | Site & Sample ID | Location | Water depth (m) | Core length (m) | Description/ Additional Info | Analyses | Sampling Resolution |
|---------|----------------|----------------|------------------|--|-----------------|-----------------|---|-------------|---|
| 14PL001 | -50° 43'03.8" | 166° 10' 17 " | 14G1 | Norman Inlet | 46.6 | – | Grey fine sand | FI | – |
| 14PL001 | -50° 44' 18.4" | 166° 07' 25.1" | 18G1 | Hanfield Inlet | 45.8 | – | Dark brown silt and fine sand | C/N | – |
| 14PL001 | -50° 44' 14.8" | 166° 07' 53.4" | 19G1 | Hanfield Inlet | 49.7 | – | Dark brown silt | C/N | – |
| 14PL001 | -50° 44' 13.7" | 166° 07' 58.9" | 20G1 | Hanfield Inlet | 53.5 | – | Dark brown silt | C/N | – |
| 14PL001 | -50° 42' 54" | 166° 06' 14.3" | 35G1 | Norman Inlet | 31.7 | – | Brown mud | FI | – |
| 14PL001 | -50° 44' 19.1" | 166° 07' 21.4" | 36G1 | Hanfield Inlet | 44.5 | – | Dark brown silt | FI | – |
| 14PL001 | -50° 44' 19.4" | 166° 07' 20.8" | 36B2 | Hanfield Inlet | 37.1 | 0.1 | 2 cores subsampled | C/N, FI | Every cm |
| 14PL001 | -50° 44' 19.2" | 166° 07' 21" | 36P4 | Hanfield Inlet | 44.4 | 5.7 | Dark brown silt and fine sand | PP, C/N, FI | Every 5cm for C/N and every 10cm for FI |
| 14PL001 | -50° 44' 14.1" | 166° 07' 56.2" | 39G1 | Hanfield Inlet | 51.8 | – | Dark brown silt and fine sand | FI | – |
| 14PL001 | -50° 44' 14.5" | 166° 07' 56.2" | 39P4 | Hanfield Inlet | 52.3 | 5.53 | Dark brown silt and fine sand and dark clay/ silt | PP | – |
| 14PL001 | -50° 42' 54" | 166° 06' 10.8" | CTD_001 | Norman Inlet | 43.5 | – | Site 35 | WI, C/N | |
| 14PL001 | -50° 44' 19.2" | 166° 07' 21" | CTD_002 | Hanfield Inlet | 44.5 | – | Site 36 | WI, C/N | |
| 14PL001 | -50° 44' 8.4" | 166° 12' 28.8" | CTD_003 | Open ocean (between Hanfield and Norman) | 67 | – | – | WI, C/N | – |
| 14PL001 | -50° 44' 18.6" | 166° 07' 22.2" | CTD_004 | Hanfield Inlet | 40 | – | Site 36 | WI, C/N | |
| 15PL001 | -50°42'54" | 166°06'54" | CTD_006 | Norman Inlet | | – | – | WI | |
| 15PL001 | -50°44'28" | 166°07'81" | CTD_007 | Hanfield Inlet | | – | – | WI | |



Table 2. Locations of surface sediment samples and accompanying bottom water oxygen ($\delta^{18}\text{O}_w$) and carbon ($\delta^{13}\text{C}_{\text{DIC}}$) stable isotope measurements. Expected oxygen isotopic composition of calcite precipitated in equilibrium with $\delta^{18}\text{O}_w$ ($\delta^{18}\text{O}_{\text{foram}}$) for a given temperature was calculated using the equation from Marchitto et al., 2014 ($\delta^{18}\text{O}_{\text{foram}} - \delta^{18}\text{O}_w(\text{VSMOW}) + 0.27 = -0.225T + 3.50$).

| Cruise | CTD | Site/sample | Fjord | Height of measurement above substrate (m) | $\delta^{18}\text{O}_w$ (‰) (SMOW) | $\delta^{13}\text{C}_{\text{DIC}}$ (‰) (VPDB) | Temperature (°C) | $\delta^{18}\text{O}_c$ (‰) (VPDB) |
|---------|---------|------------------|----------|---|------------------------------------|---|------------------|------------------------------------|
| 14PL001 | CTD_001 | 35G1 | Norman | 1 | -0.26 | 0.64 | 10.55 | 0.60 |
| 14PL001 | CTD_002 | 36G1, 36B2, 39G1 | Hanfield | 4 | -0.1 | 1.21 | 10.55 | 0.76 |
| 14PL001 | CTD_004 | 36G1, 36B2, 39G1 | Hanfield | 8.5 | -0.24 | 0.03 | 10.5 | 0.63 |
| 15PL001 | CTD_006 | - | Norman | | 0.31 | - | 10.4 | 1.31 |
| 15PL001 | CTD_007 | - | Hanfield | | 0.29 | - | 9.9 | 1.28 |

855

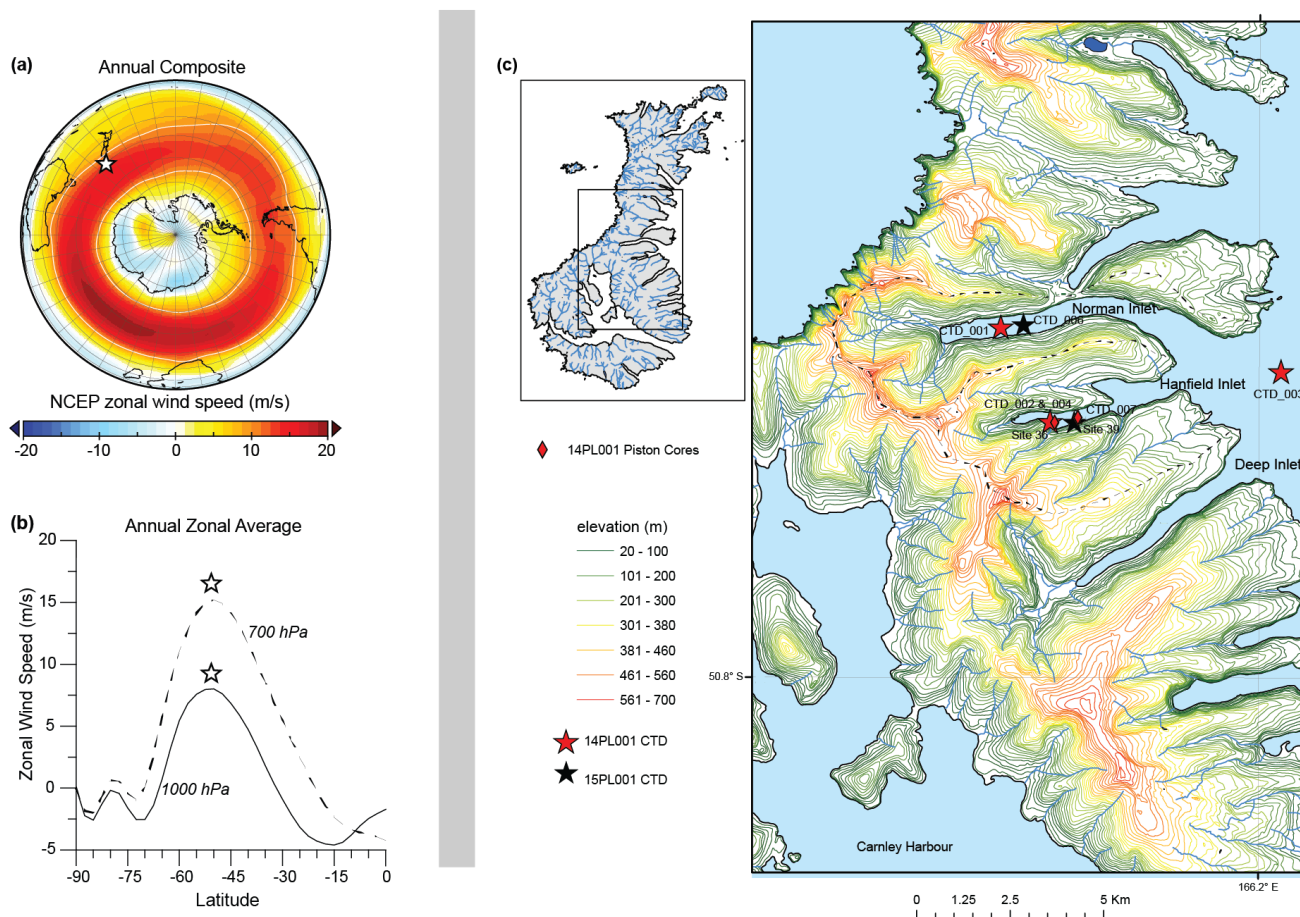
Table 3. Average benthic foraminiferal oxygen and carbon isotopic compositions ($\delta^{18}\text{O}_{\text{foram}}$ and $\delta^{13}\text{C}_{\text{foram}}$) from grab and core-top sediments collected from Hanfield (sites 36 and 39) and Norman Inlet (site 35) in 2014.

| Species | Number of duplicate measurements | Average $\delta^{18}\text{O}_{\text{foram}}$ (‰) VPDB | Standard deviation for $\delta^{18}\text{O}_{\text{foram}}$ (‰) VDPB | Av $\delta^{13}\text{C}_{\text{foram}}$ (‰) (VPDB) | Standard deviation for $\delta^{13}\text{C}_{\text{foram}}$ (‰) VDPB |
|---|----------------------------------|---|--|--|--|
| <i>B. marginata</i> f. <i>marginata</i> | 5 | 1.64 | 0.10 | -0.34 | 0.31 |
| <i>Cibicides</i> spp. | 3 | 1.25 | 0.07 | 1.67 | 0.12 |
| <i>N. flemingi</i> | 5 | 2.00 | 0.21 | -0.99 | 0.49 |
| <i>Q. seminula</i> | 6 | 1.60 | 0.22 | -0.11 | 0.31 |
| <i>T. angulosa</i> | 6 | 1.66 | 0.16 | 0.49 | 0.25 |

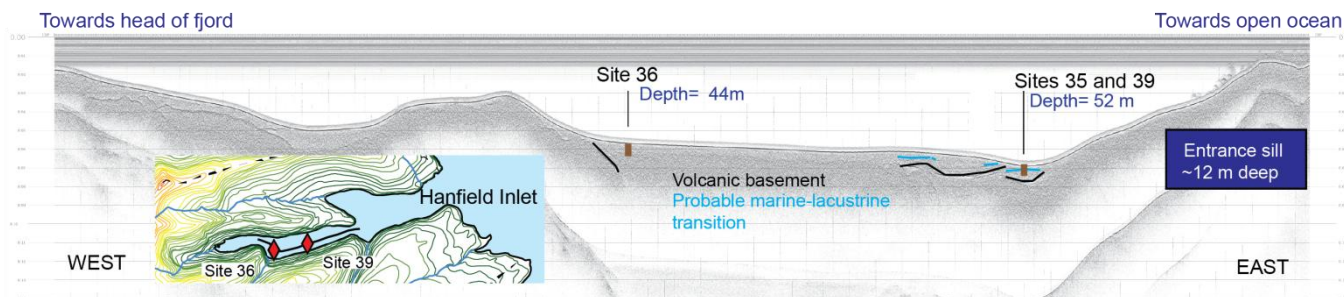
860

Table 4. Median Probability Ages and associated error for eight AMS radiocarbon-dated terrestrial organic macrofossil fragments from 36P4, Hanfield Inlet. Radiocarbon years were converted to cal yr BP using SHCal13 (Hogg et al., 2013) in Calib 7.0.4 (Stuvier and Reimer, 2003).

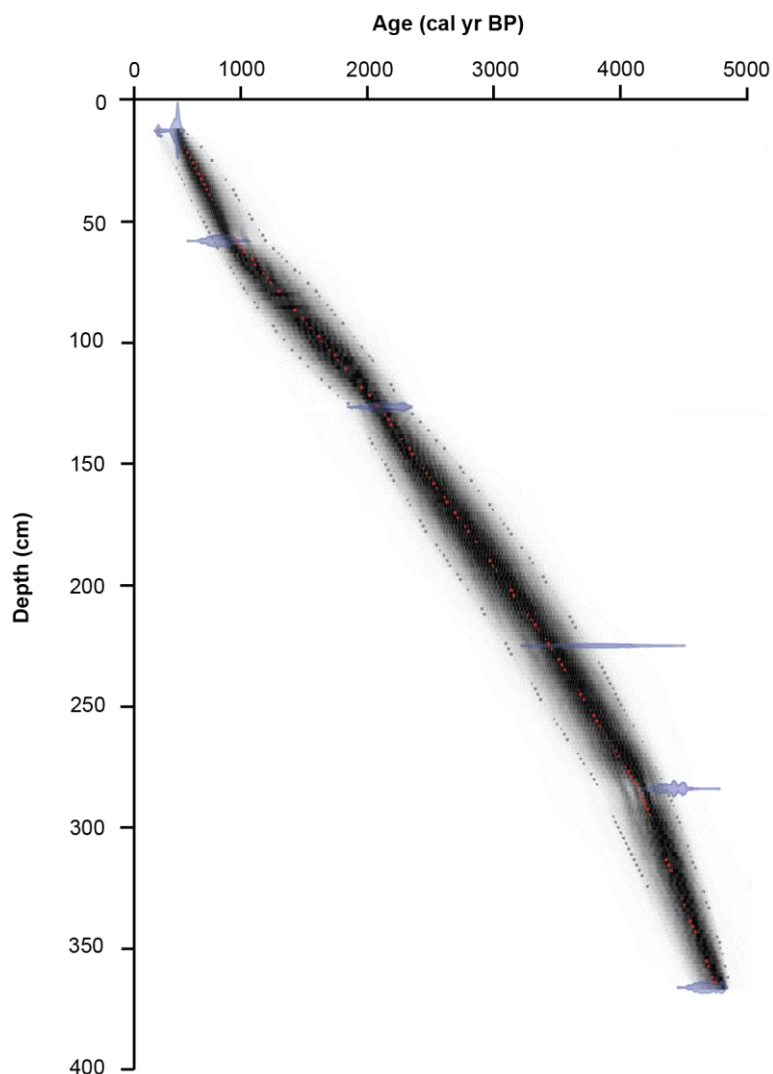
| Core ID | Depth (cm) | 14C years | Median Probability Age (cal yr BP) | Lower 20 | Upper 20 |
|---------|------------|------------|------------------------------------|----------|----------|
| 36P4 | 12.5 | 470 ± 30 | 497 | 340 | 526 |
| 36P4 | 58 | 960 ± 80 | 831 | 685 | 956 |
| 36P4 | 126.5 | 2180 ± 70 | 2136 | 2017 | 2299 |
| 36P4 | 225 | 3560 ± 210 | 3820 | 3512 | 4089 |
| 36P4 | 284 | 4000 ± 40 | 4419 | 4255 | 4525 |
| 36P4 | 366 | 4190 ± 30 | 4691 | 4539 | 4827 |
| 36P4 | 451 | 5360 ± 140 | 6095 | 5942 | 6272 |
| 36P4 | 542.5 | 5315 ± 30 | 6060 | 5938 | 6180 |



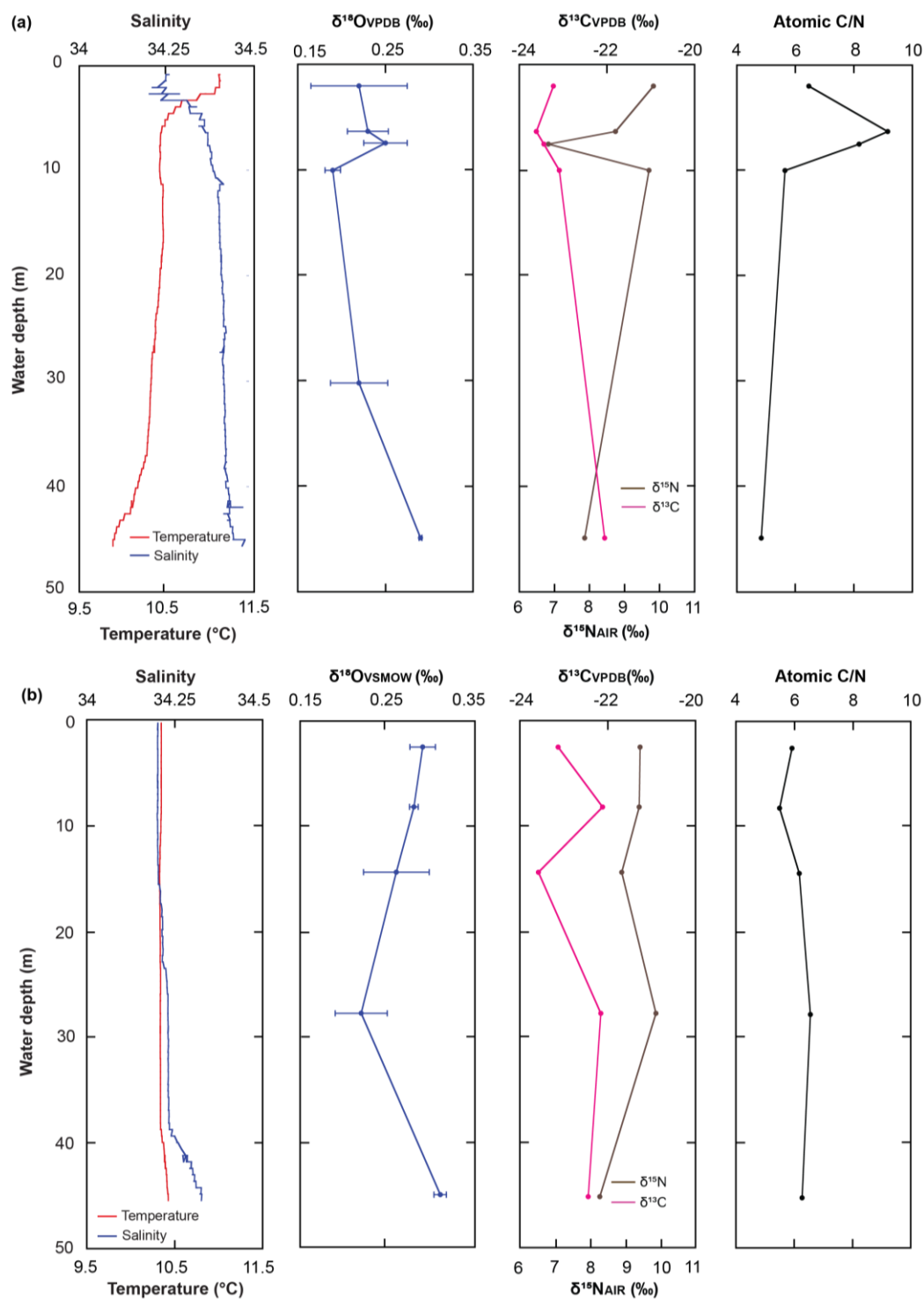
865 **Figure 1.** (a) and (b) Annual composite 700 hPa zonal wind speed. Data sourced from NCEP reanalysis (Kalnay, 1996). The star denotes the position of New Zealand's subantarctic Auckland Islands (51° S, 166° E). (c) Detailed view of piston coring and CTD locations at the Auckland Islands. Data were collected in February of 2014 (14PL001) and 2015 (15PL001). Thick black lines indicate the catchment areas for Norman and Hanfield Inlets.



870 **Figure 2.** Seismic section of Hanfield Inlet, location of line shown on inset map. The fjord contains two sub-basins and has an entrance sill ~12 m deep. Black reflectors represent the transition to underlying glacial sediments, and pale blue reflectors are probably the marine to lacustrine transition, which was sampled in core 39P4 (site 39). The core used for paleoclimate reconstruction is 36P4 (site 36).



875 **Figure 3.** A posterior age-depth model for piston core 36P4 (grey field) calculated using Bayesian interpolation of six ^{14}C dates (from terrestrial organic macrofossil fragments) from core 36P4 from Hanfield Inlet. Age-depth model was constructed using Bacon software (Blauuw and Christen, 2011). See text for model input parameters. Radiocarbon ages were calibrated to cal yr BP using SHCal13 (Hogg et al., 2013). Red dots indicate the weighted mean calibration age and the grey dots represent the 95% confidence interval.

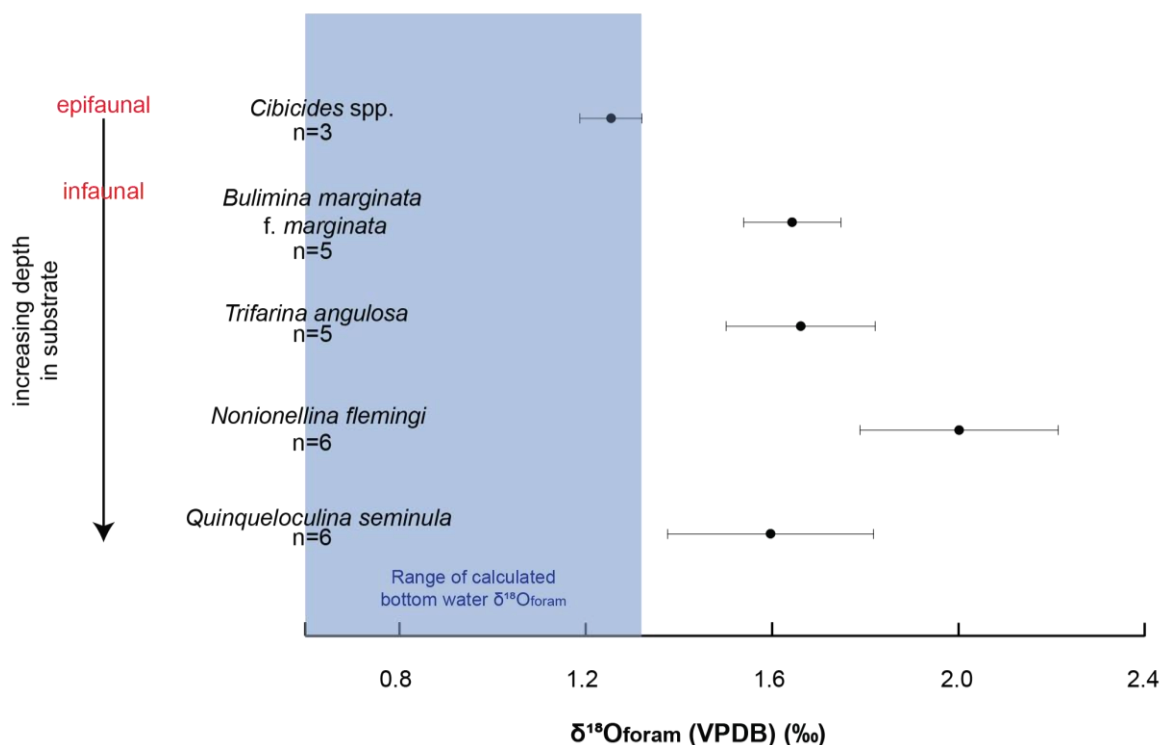


880 **Figure 4. Modern fjord water temperature, salinity, $\delta^{18}\text{O}$ and $\delta^{13}\text{C}$, $\delta^{15}\text{N}$ & molecular C/N of acidified particulate organic matter (POM) for a) Hanfield Inlet (CTD_007) and b) Norman Inlet (CTD_006). Both water profiles were sampled in February 2015,**



885

during dry (a) and rainy (b) conditions. Temperature is slightly elevated and salinity is slightly depressed in the upper 4 m of the water column during fair weather, and $\delta^{18}\text{O}$ is depleted in the upper ~10 m. POM $\delta^{15}\text{N}$ shows an overall increase with depth, while $\delta^{13}\text{C}$ and molecular C/N show a decrease. During rainy conditions, temperature and salinity are largely homogenous through the water column, but show a slight increase at depth, and particulate $\delta^{15}\text{N}$ and $\delta^{13}\text{C}$ are variable. Molecular C/N remains relatively unchanged with depth. Error bars are 2σ for duplicate measurements. For CTD data from 2014, see Table S1.



890

Figure 5. Deviation of benthic foraminiferal oxygen isotopic composition ($\delta^{18}\text{O}_{\text{foram}}$) from calculated equilibrium according to Marchitto et al., 2014 ($\delta^{18}\text{O}_{\text{foram}} - \delta^{18}\text{O}_w(\text{VSMOW}) + 0.27 = -0.225T + 3.50$) for five species from Hanfield and Norman Inlets. This equation, derived for *Cibicides* spp. is indistinguishable from the temperature equation from O'Neil and Kim 1997 for inorganic calcite, so is considered valid for all species. Range of expected $\delta^{18}\text{O}_{\text{foram}}$ encompasses the entire range of measured summer fjord bottom water temperatures and $\delta^{18}\text{O}_w$ from Hanfield and Norman Inlets (Tables 2 and 3).

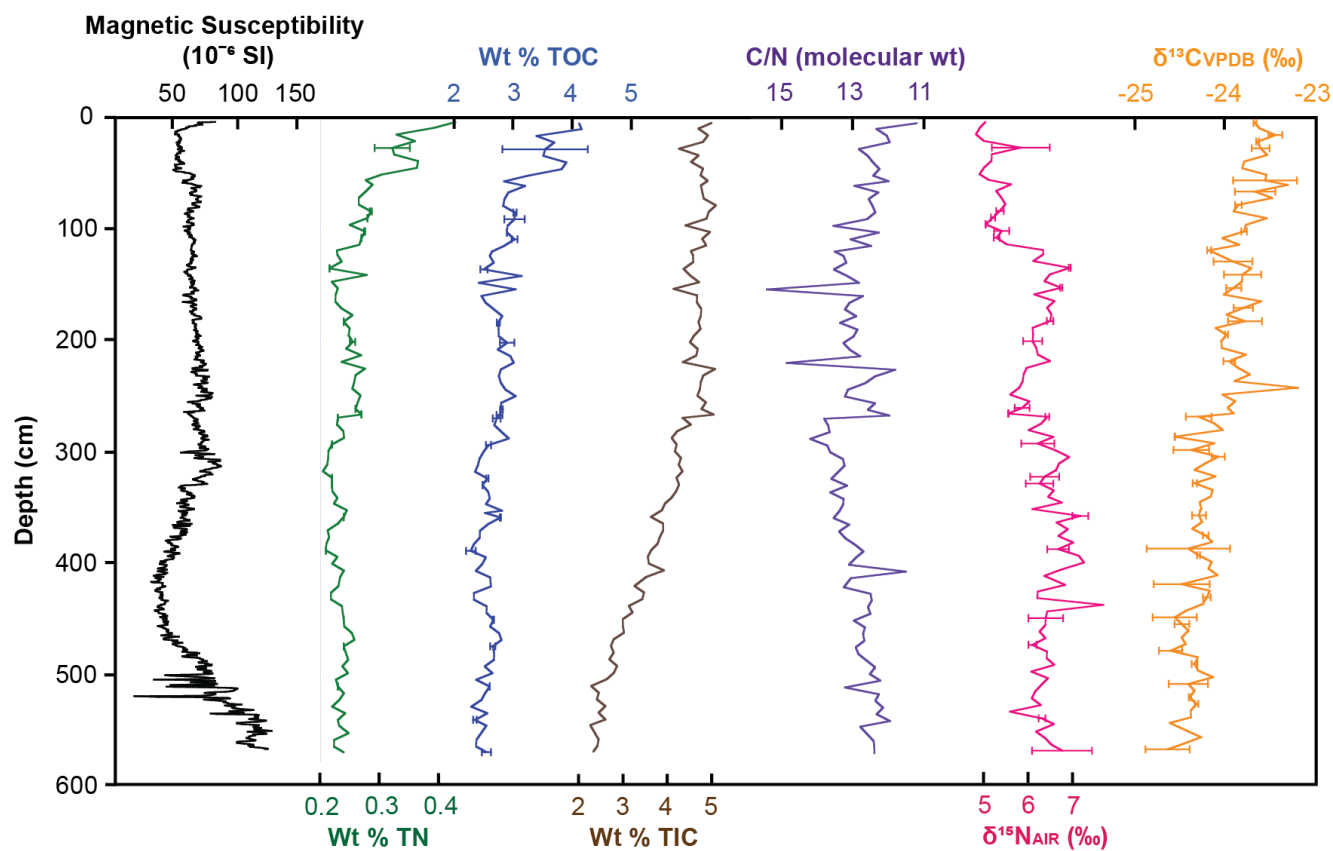
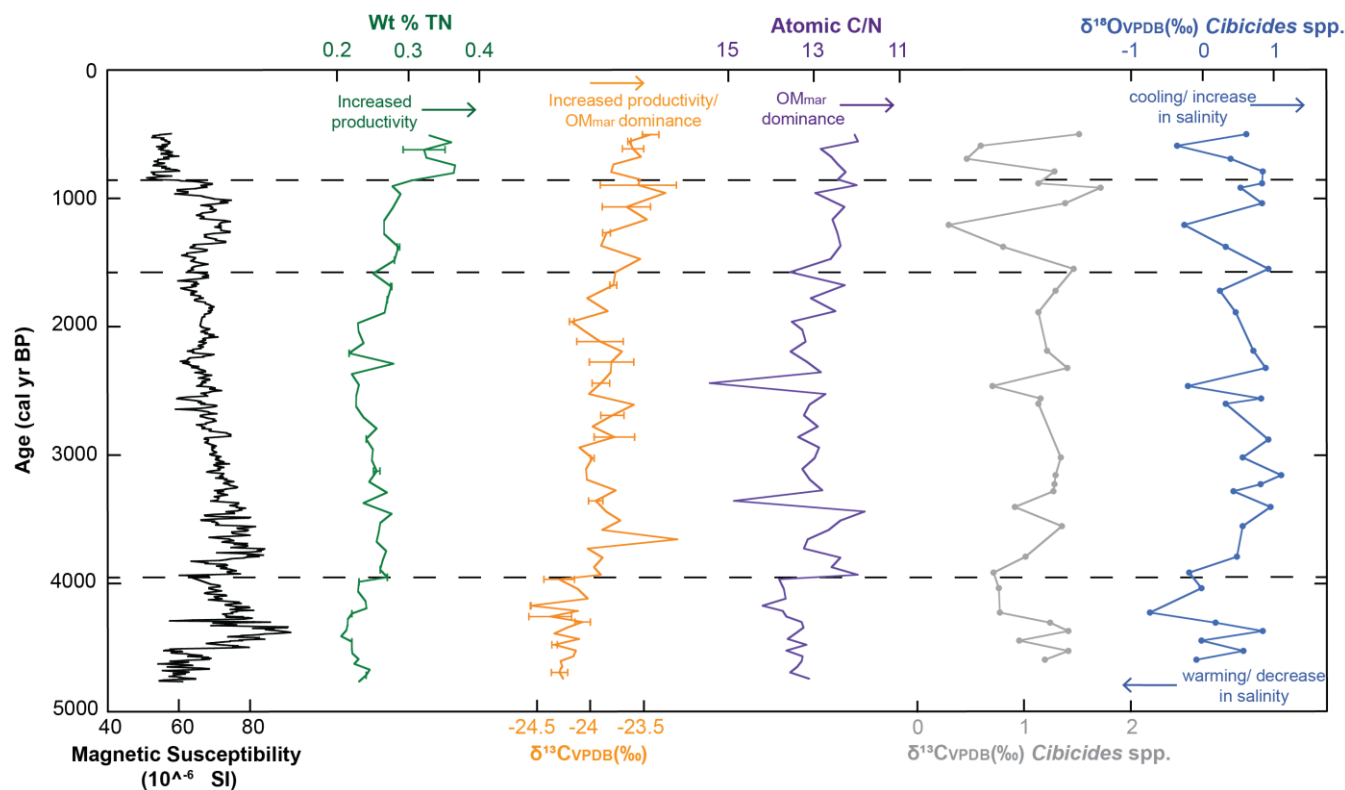
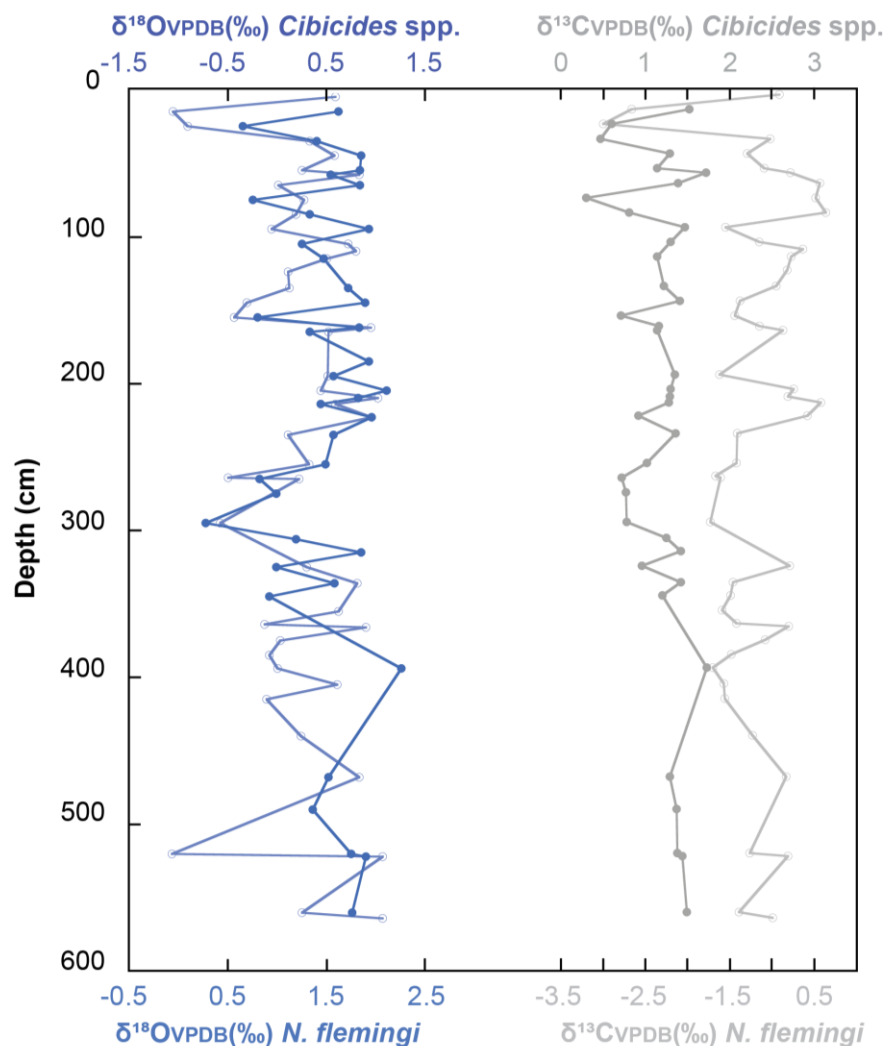


Figure 6. Downcore parameters against depth, 36P4, Hanfield Inlet: magnetic susceptibility, wt % nitrogen (TN), wt % organic carbon (TOC), wt % carbonate (TIC), $\delta^{13}\text{C}$, $\delta^{15}\text{N}$ and molecular C/N of bulk sediment. Error bars are 2σ for duplicate measurements.

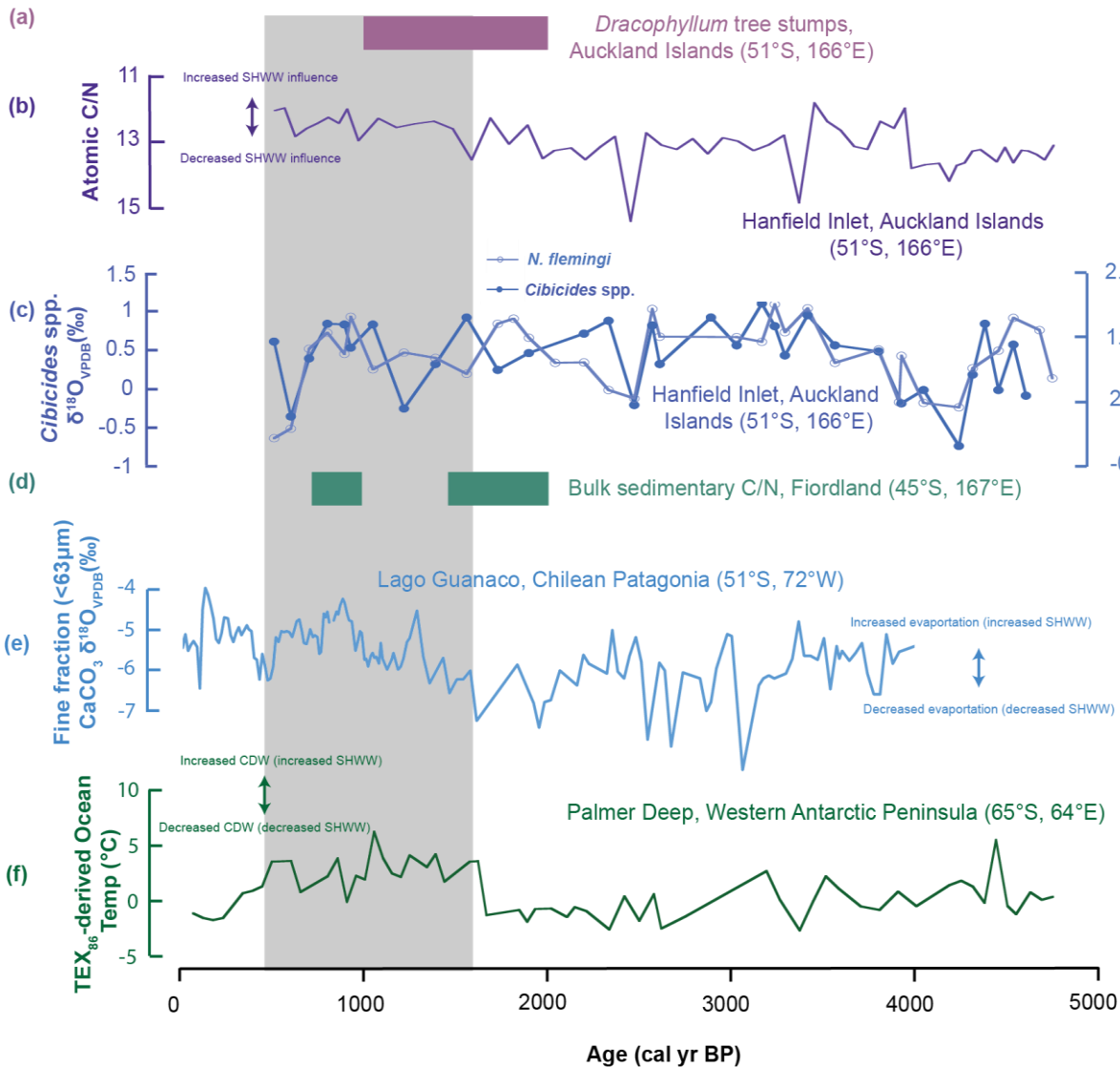
895



900
 905
Figure 7. Downcore parameters against age, 36P4, Hanfield Inlet: magnetic susceptibility (MS), wt % nitrogen (TN), $\delta^{13}\text{C}$ and molecular C/N of bulk sediment, and $\delta^{13}\text{C}$ & $\delta^{18}\text{O}$ of benthic foraminifer *Cibicides* spp. Error bars are 2σ for replicate measurements (see text for stable foraminifer isotope error). The dashed horizontal lines at ~4,000, 1,600 and 900 yr BP break the core into three sections based on prominent shifts across multiple proxies. From 4,000-1,600 yr BP, fjord conditions are relatively stable, as indicated by relatively unchanging MS, wt % TN, $\delta^{13}\text{C}$ and molecular C/N. This interval is characterised by more negative $\delta^{13}\text{C}$ and higher C/N, indicating a higher contribution from OM_{terr}, increased stratification and decreased SHWW influence at this time. From 1,600-900 yr BP, increasing wt % TN, more positive $\delta^{13}\text{C}$ and more negative C/N indicates a shift to OM_{mar} dominance, signifying a strengthening of the SHWW at this time. Paired fluctuations in benthic foraminifer $\delta^{13}\text{C}$ and $\delta^{18}\text{O}$ demonstrate increased variability during this period, associated with westerly-wind driven changes in shelf hydrography. From 900-500 yr BP, a decrease in MS accompanied by an increase in wt % TN indicates an increase in productivity (also reflected by more positive $\delta^{13}\text{C}$), rather than strengthened winds at this time.



910 Figure 8. Downcore variations in $\delta^{18}\text{O}_{\text{foram}}$ for oxygen (left) and carbon (right) isotopes, 36P4, Hanfield Inlet. Solid circles represent *Cibicides* spp. and open circles represent *N. flemingi*. Blue indicates $\delta^{18}\text{O}$ and grey is $\delta^{13}\text{C}$. Note disturbance in this core at ~420cm. Both species show similar trends and similar magnitude of $\delta^{18}\text{O}_{\text{foram}}$ variation in downcore, although *N. flemingi* exhibits more positive values relative to *Cibicides* spp. (due to species-specific vital offsets; see Fig. 5). Both the trends and absolute magnitude of isotopic shifts for $\delta^{13}\text{C}_{\text{foram}}$ differ between the two species. *N. flemingi* exhibits more negative $\delta^{13}\text{C}_{\text{foram}}$ with a higher
 915 range of values, whereas *Cibicides* spp. exhibits more positive $\delta^{13}\text{C}_{\text{foram}}$ with a lower range.



920 **Figure 9.** Comparison of the current record of SHWW variability at the Auckland Islands to other Southern Hemisphere records. Horizontal coloured bars indicate periods of intensified westerly winds and the vertical grey bar represents late Holocene intensification of the winds in several areas. (a) Tree-line reconstruction using *Dracophyllum* tree stumps from the Auckland Islands (Turney et al., 2016). (b) Bulk sedimentary C/N from Hanfield Inlet, Auckland Islands. (c) Benthic foraminifer (*Cibicides* spp.) $\delta^{18}\text{O}$ from Hanfield Inlet, Auckland Islands. (d) Bulk sedimentary C/N from Fiordland, New Zealand (Knudson et al., 2011). (e) Fine fraction (<63 μm) biogenic carbonate $\delta^{18}\text{O}$ from Lago Guanaco, Chilean Patagonia (Moy et al., 2008). (f) TEX_{86} -derived upper ocean temperatures (0-200 m) from Palmer Deep, western Antarctic Peninsula (Shevenell et al., 925 2011).